Environmental Pollution 328 (2023) 121612

Contents lists available at ScienceDirect

Environmental Pollution

journal homepage: www.elsevier.com/locate/envpol

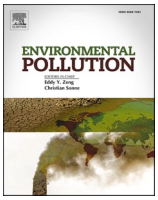

Firework smoke: Impacts on urban air quality and deposition in the human respiratory system☆

Imre Salma [a,*], Árpád Farkas [b], Tamás Weidinger [c], Miklós Balogh [d]

[a] Institute of Chemistry, Eötvös Loránd University, Budapest, Hungary
[b] Center for Energy Research, Budapest, Hungary
[c] Department of Meteorology, Institute of Geography and Earth Sciences, Eötvös Loránd University, Budapest, Hungary
[d] Department of Fluid Mechanics, Faculty of Mechanical Engineering, Budapest University of Technology and Economics, Budapest, Hungary

ARTICLE INFO

Keywords:
Air pollution
Fireworks
Particle number concentration
Size distribution
Plume dispersion
Inhalation

ABSTRACT

Particle number concentrations and size distributions resulting from the firework displays held in Budapest, Hungary every year on St. Stephen's Day were studied over a period of seven years. In the year most impacted, the total particle number concentration reached its peak measured level of 369×10^3 cm^{-3} 5 min after the end of the display, and returned to the pre-event state within 45 min. The fireworks increased hourly mean concentrations by a factor of 5–6, whereas the concentrations in the diameter range of 100–1000 nm, in which the magnitude of the increase was the greatest, were elevated by a factor of 20–25. An extra particle size mode at 203 nm was manifested in the size distributions as result of the fireworks. The PM_{10} mass concentrations at peak firework influence and as 1-h mean increased 123 and 58 times, respectively, relative to the concentration before the display. The smoke was characterised by a relatively short overall atmospheric residence time of 25 min. Spatiotemporal dispersion simulations revealed that there were substantial vertical and horizontal concentration gradients in the firework plume. The affected area made up a large part of the city. Not only the spectators of the display at the venue and nearby areas, but the population located further away downwind of the displays and more distant, large and populous urban quarters were affected by the plume and its fallout. The fireworks increased the deposition rate in the respiratory system of females by a factor of 4, as a conservative estimate. The largest surface density deposition rates were seen in the segmental and sub-segmental bronchi, which represents an excessive risk to health. Compared to adults, children were more susceptible to exposure, with the maximum surface density deposition rates in their case being three times those of adults in the trachea.

1. Introduction

Many cultural and festive events all around the world are accompanied by spectacular firework displays. As result of the rapid combustion, fireworks locally generate very high concentrations of pollutant gases (such as SO_2, NO, NO_2 and CO), organic xenobiotics (such as polychlorinated dibenzo-p-dioxins and dibenzofurans), and smoke (Bach et al., 2007; Lin, 2016; Sun et al., 2017; Hickey et al., 2020; Fu et al., 2021). The relatively high abundance of hygroscopic substances in firework-generated particles can also produce haze at higher relative humidity (RH) (Cao et al., 2018). The smoke is dispersed in the air both during and after the firework activity (Holmes and Morawska, 2006). The resulting plume can have a considerable negative impact on local air quality (Moreno et al., 2007, 2010; Barman et al., 2008; Vecchi et al., 2008; Joly et al., 2010; Sarkar et al., 2010; Seidel and Birnbaum, 2015; Dickerson et al., 2017; Greven et al., 2019; Singh et al., 2019; Mousavi et al., 2021). The fallout from the plume created from firework displays becomes deposited on surfaces, such as soil, roads, parks, surface waters and other outdoor recreation areas even for longer periods after the display (Sijimol and Mohan, 2014; Baranyai et al., 2014; Yang et al., 2019). Other aspects and impacts of fireworks, including the consequences they have on human health, the biosphere and the environment are outlined in Sect. S1.

Studies on the atmospheric concentrations of firework-related hazardous aerosol substances are limited by the time resolution of sampling devices and by the smallest sample amounts needed for chemical

☆ This paper has been recommended for acceptance by Admir Créso Targino.

* Corresponding author.
E-mail address: salma.imre@ttk.elte.hu (I. Salma).

https://doi.org/10.1016/j.envpol.2023.121612
Received 9 November 2022; Received in revised form 3 April 2023; Accepted 8 April 2023
Available online 14 April 2023

analyses. However, high-resolution time-of-flight aerosol mass spectrometers (HR-ToF-AMS) are not subjected to these limitations (Drewnick et al., 2006; Jiang et al., 2015; Zhang et al., 2019). As far as particle number concentrations and size distributions are concerned, these values may also be determined at high time resolution (Wehner et al., 2000; Mönkkönen et al., 2004; Zhang et al., 2010). Moreover, the relatively short atmospheric residence time of sub-micrometer particles is beneficial for investigating the dynamics of the sources and the transformation processes. The related PM mass can be determined from the particle number size distributions, whereas chemical composition can be estimated from parallel or auxiliary experiments. To date, most measurement results have been obtained in Asia (mainly in China and India), while data from Europe are sparse (Cao et al., 2018).

The largest organised firework display in Hungary takes place in the capital, Budapest on the national holiday of 20 August, on Saint Stephen's Day. The National Air Quality Network has no automatic monitoring station located in the source area. However, aerosol and meteorological measurements have been performed continuously for research purposes near to the firework display for more than 10 years (Salma et al., 2021a).

The main objectives of the present work are to characterise and quantify the firework smoke and its transformation processes in Budapest in terms of particle number and PM mass concentrations. Specifically, we report and explain the changes in particle number size distributions, determine and interpret the atmospheric residence time of smoke particles, and assess the contribution of the fireworks to local air pollution. Additional goals were to model the spatiotemporal dispersion of particles using computational fluid dynamics (CFD), and to estimate and discuss the exposures to and health risk from the firework plume using stochastic respiratory deposition modelling.

2. Methods

2.1. The durations and locations of firework displays and measurements

The data measured at the Budapest platform for Aerosol Research and Training (BpART) Laboratory on St Stephen's Day in 2014, 2015, 2016, 2017, 2021 and 2022 were evaluated. The specific date is 20 August, but the firework display was postponed in 2022 to 27 August because of a bad weather forecast. We have no aerosol data for that specific day in 2018 and 2019. In 2020, there was no firework display due to the COVID-19 pandemic, but this case was also included to the study for checking and verification purposes. The firework displays in 2021 and 2022 were the most monumental events (even in Europe) (Table S1). The meteorological conditions in 2021 favoured the detection of the smoke plume at the fixed measurement site better than in the other years (Sect. 3.5). Therefore, this particular case was used in further extensive modelling calculations.

All the fireworks in the displays were set off over the river Danube. An overview on the spatial extent, the number of individual fireworks and the locations of the launching devices is given in Sect. S2. The displays started at 21:00 local daylight-saving time (LDST = UTC+2) and lasted for 30–35 min. Many spectators gather on the riverbanks and beyond to enjoy the fireworks and an estimated 700 thousand spectators watched the fireworks at the venue in person in 2021 (Duna Media Service Provider, 2022).

The BpART Lab is situated in central Budapest (N 47° 28′ 30″, E 19° 3′ 45″, 115 m above mean sea level) (Salma et al., 2016) ca. 85 m from the Danube River. This location represents an average atmospheric environment for the city centre. In addition, according to the prevailing wind direction, it is downwind of the fireworks. A map indicating the source area in the city centre over the years together with the position of the fixed measurement site is depicted in Fig. 1.

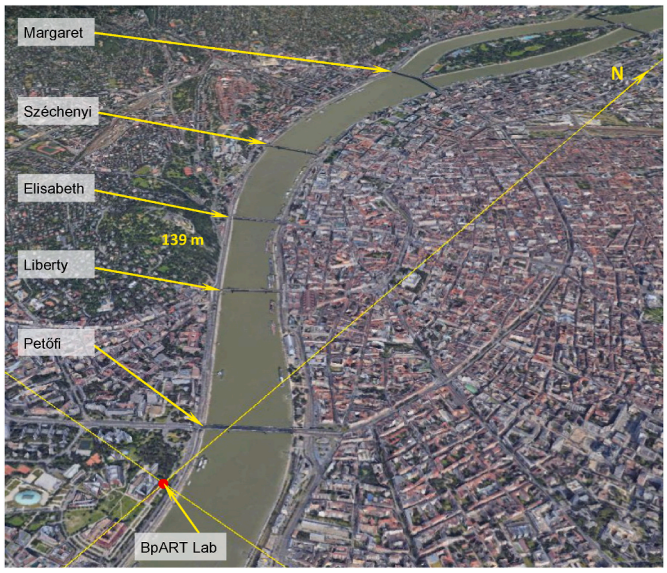

Fig. 1. The firework source areas above the Danube River in central Budapest constrained by bridges as detailed in Table S1 and the location of the fixed measurement site of the BpART Lab (red dot). The long and the short intersecting yellow lines mark the lines of longitude and latitude. The highest relative elevation in the area (Gellért Hill) is also indicated. Source: Google Maps. (For interpretation of the references to colour in this figure legend, the reader is referred to the Web version of this article.)

2.2. Measurements

The particle number concentrations and size distributions were obtained using a condensation particle counter (CPC) and a differential mobility particle sizer (DMPS). Their sampling inlets were set up at heights between 12 and 13 m above street level. The former instrument (type CPC3752, manufacturer TSI, USA) was operated with an aerosol inlet flow of 1.5 L min^{-1} and recorded total concentrations of particles with a diameter $d > 4$ nm (Salma et al., 2021b). Mean particle number concentrations (N_{CPC}) with a time resolution of 1 s or 1 min were extracted from the instrument's database. The DMPS was a flow-switching-type system, which measured the particle number concentrations in an electrical mobility diameter range from 6 to 1000 nm of particles in the dry state (RH<30%) in 27 size channels with a time resolution of 8 min (Salma et al., 2016, 2021a). The DMPS and CPC measurements were performed according to international technical standards (Wiedensohler et al., 2012; Mikkonen et al., 2020; Salma et al., 2021b).

Air temperature (T), RH, wind speed (WS) and wind direction (WD) were recorded on site using standardised meteorological sensors (instrument type HD52.3D17, manufacturer Delta OHM, Italy) with a time resolution of 1 min. In addition, WS and WD data above the rooftop level of the building complex at a height of 42 m above street level were also obtained (instrument types WAA15A and WAV15A, manufacturer Vaisala, Finland) with a time resolution of 10 min. The height of the temperature inversion layer (TIL) and the WS and WD data at its top level were derived from radiosonde data obtained from the Hungarian Meteorological Service (station no. 12843) ca. 10 km from the BpART Lab at 24:00 UTC.

2.3. Data treatment

Particle number size distribution surface (contour) plots jointly showing the variation in particle diameter and particle number concentration density over time were derived from the inverted DMPS data for all days (Salma et al., 2011a). Particle number concentrations in the diameter ranges from 6 to 1000 nm ($N_{6–1000}$), from 6 to 100 nm ($N_{6–100}$),

and from 100 to 1000 nm ($N_{100–1000}$) were obtained from the size distributions. The effects of the fireworks on the actual air quality were quantified by comparing sample mean concentrations for 1 h before the event (m_{before}, from 20:00 to 21:00), for 1 h during the event and during the time of the direct impacts (m_{during}, from 21:00 to 22:00) and for 1 h well after the end of the show (m_{after}, from 22:30 to 23:30). The mean concentrations were compared using their ratios (r_{before}), i.e.

$$r_{before} = \frac{m_{during}}{m_{before}} . \quad (1)$$

The interpretation of ratios, however, depends on the absolute magnitude of their variables, so an additional metric, the value Z was calculated, i.e.

$$Z_{before} = \frac{m_{during} - m_{before}}{SD} . \quad (2)$$

This expresses the difference between the means with regard to the ordinary fluctuation in the data set. The sample standard deviation (SD) was calculated for the actual day excluding the extended firework interval of 21:00–22:30. The value Z is interpreted as the reliability or confidence of the related ratio. The characteristics r_{after} and Z_{after} for the intervals during and after the firework display were calculated in analogy with Eqs. (1) and (2).

The particle number size distributions were fitted using the DoFit algorithm (Hussein et al., 2004), and their modes were characterised by modal concentration (N_m), particle number median mobility diameter (NMMD) and geometric standard deviation (GSD). Coagulation scavenging efficiencies for particles with diameters d of 6, 10, 25, 100 and 200 nm ($CoagS_d$) and condensation sink (CS) for low-volatility vapour molecules onto the existing aerosol particles were computed using conventional aerosol mechanics (Kulmala et al., 2001, 2012). The hygroscopic growth of particles (due to uptake of moisture from the air) in subsaturated RH conditions was not taken into account since this can sensitively depend on the chemical composition of the particles, which is expected to be unusual in this case compared to atmospheric aerosol.

2.4. Modelling

Further modelling calculations were carried out for a selected year, namely 2021, since the effects of the fireworks at the measurement location were the most clearly recognisable in this particular case.

The dispersion of the firework pollutants was assessed with CFD simulations using an incompressible approach and Lagrangian particle tracking. To describe the effect of turbulence on the flow field and dispersion, the k-ε Reynolds-averaged Navier−Stokes model was used with those modifications applied to the model suggested for atmospheric turbulence (Balogh et al., 2012; Balogh and Parente, 2015). The complex urban texture of the studied area (Figs. 1 and S1a) was discretised with a high-resolution computational mesh (Fig. S1b). The development process together with some additional aspects and details of the model are described in Sect. S3.

Depositions of aerosol particles in the whole human respiratory system, in its major anatomical parts, namely in the extra-thoracic (ET; or oro-naso-pharyngeal-laryngeal) region, the tracheobronchial (TB) tree and the acinar (AC) region and in airway generations were assessed by an advanced version of the stochastic lung model IDEAL (e.g. Balásházy et al., 2007; Farkas et al., 2022). Particle number size distributions and total concentrations in the firework plume were utilised in the computations using the electrical mobility diameter representation (Salma et al., 2015). A healthy Caucasian-type female adult and a 5-year-old child performing reference seated physical activity were considered. Further aspects and details of the respiratory system deposition model are described in Sect. S4 and can be found in earlier publications (e.g. Hofmann, 2011; Salma et al., 2002b).

3. Results and discussion

There were no sudden or substantial meteorological changes or extraordinary aerosol sources active during the investigated days (Table S3). They suggest that the observed and derived aerosol properties, tendencies and changes were primarily caused by and related to firework displays. The contour plot of particle number size distribution for the most impacted year of 2021 is shown in Fig. 2, whereas the plots for the other years are displayed in Figs. S4 and S5. The plume at the BpART Lab after 21:00 was easily perceptible and evidently recognisable in the measurements from 2021 to 2022, and it was also detected in 2016 and 2017. However, the plume could not be distinguished in 2014 or 2015. The reasons for the plumes being identified or not, lay in the local meteorology, including particularly the WD, WS and TIL height (Sect. S5).

3.1. Time series of total particle number concentrations

The time evolution of N_{CPC} in 2021 with a resolution of 1 min is shown in Fig. 3. The median particle number concentration until the beginning of the firework display was 12×10^3 cm^{-3}. This is somewhat higher than, but comparable to the daily medians in central Budapest (Salma and Németh, 2019). The concentration exhibited considerable variability (from 4.9×10^3 to 36×10^3 cm^{-3}), which is an ordinary feature of particle number concentrations in cities. Sunset was at 20:47. The first sudden considerable increment at 20:00 could be related to ordinary changes and fluctuations.

The first pyrotechnic devices were launched at 21:06. The sudden concentration increment at 21:15 (see also Fig. S6 with a time resolution of 1 s) is already an impact of the firework activity and was recorded at the BpART Lab approximately 9 min after the actual beginning of the display. This delay was influenced by the advection of the smoke from the source area to the measurement site (Sect. 3.5.). The time series reached its maximum of 369×10^3 cm^{-3} 4–5 min after the end of the firework activity. This concentration was larger than the mean concentration just before the event by a factor of 30 and is regarded as an extreme value in Budapest and in other European and USA cities (Kumar et al., 2014; Salma and Németh, 2019). During the concentration elevation phase, the data increased by 11×10^3 cm^{-3} every minute (which increment is comparable to the pre-existing concentration). The measured maximum may be influenced by source strength, distance between the source and receptor, and even by the local meteorology, which may vary from year to year. The structural elements of the time series (which are more apparent in Fig. S6) may be related to specific firework device types, e.g. Roman candles and waterfall fire effects that

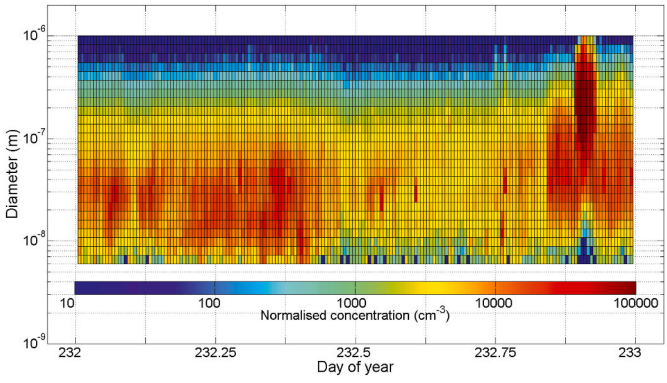

Fig. 2. Contour plot of particle number size distributions in the diameter range from 6 to 1000 nm on 20 August 2021. The normalised concentrations are expressed as dN/dlog(d). The firework display started at 21:00 LDST and lasted for ca. 30 min. Its effect appears as a dark red oval patch in the right upper part of the figure. (For interpretation of the references to colour in this figure legend, the reader is referred to the Web version of this article.)

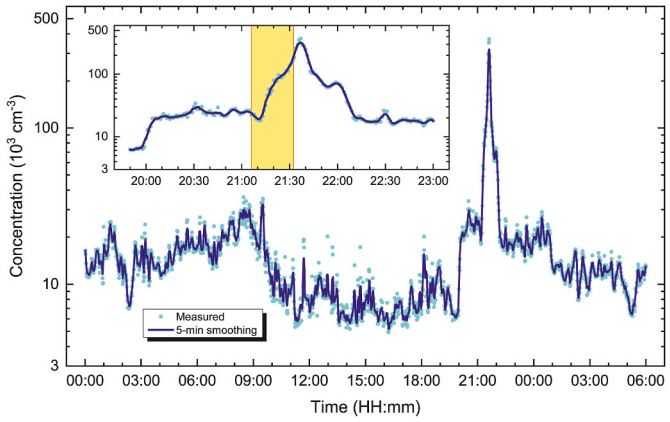

Fig. 3. Time series of total particle number concentration measured by CPC on 20 and 21 August 2021 together with its 5-min smoothing. The firework activity started at 21:06 and lasted for 26 min. The insert shows a more detailed time evolution between 19:50 and 23:00; the firework activity is indicated by a yellow band. (For interpretation of the references to colour in this figure legend, the reader is referred to the Web version of this article.)

produce large concentrations directly in the surface layer and partly to the decreased near-surface WS by the end of the display. The concentration returned to its pre-event level 40–45 min after the pyrotechnic activity.

The time evolution of total particle number concentration in 2022 was similar to that for 2021 (Fig. S7a). This exhibited a smaller maximum of 124 × 10^3 cm^{-3} and a longer plateau-type duration. In 2020 (no fireworks, Fig. S7b), the time series exhibited an ordinary diurnal pattern with variability caused by the usual daily cycling of sources and meteorological conditions and regular atmospheric fluctuations (Salma et al., 2014).

3.2. Size distributions

The time evolution of the particle number size distribution during the firework display in 2021 is shown in Fig. 4. The other distributions, particularly for 2022, were similar to this in shape, characteristics and dynamics (Fig. S8). These distributions imply that the largest concentration alterations occurred in the size range from 100 to 1000 nm. Initially, the distributions showed a rapid increase to maximum, and then, a more modest decline. The elevation phase is primarily related to

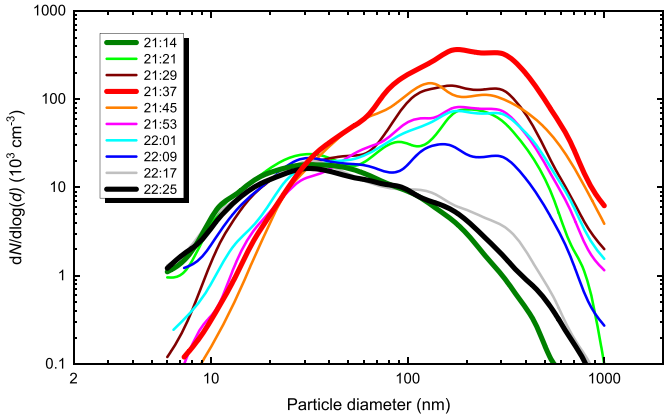

Fig. 4. Time series of the particle number size distribution from 21:14 to 22:25 for the fireworks in 2021. The distributions just before the observed firework activity (21:14), at its concentration maximum (21:37) and after it settled down to the levels before the show (22:25) are emphasised with thicker curves. The timing data refer to the end time of the 8-min measuring cycle of the DMPS system.

source intensity and smoke advection, while the decrease is mainly caused by dispersion, dilution of the plume and the transformation processes taking place inside it. The final size distribution (at 22:25 in Fig. 4) was similar to the initial curve (at 21:14).

The lines cross each other at a diameter between 30 and 40 nm. At larger values than this intersect, the concentrations were substantially and systematically higher during the entire firework event than before and after it, and varied in an arrayed manner. The situation was just the opposite below the intersection point.

At smaller values than the intersect, concentrations were substantially and systematically lower during the entire firework event than both before and after it. Furthermore, the larger the concentration elevation in the 100–1000-nm range, the smaller the concentration of particles with a diameter of 6–30 nm. The phenomenon can be also clearly seen in the corresponding contour plot (Fig. 2). This depicts the time evolution of the concentrations in the size channels below 30 nm as a structured concentration depression (blue area in the form of a peak in the bottom part of the plot) during the firework event. Aerosol mechanics can explain this phenomenon.

Coagulation of aerosol particles is especially favoured if one of the two particles possesses a larger surface area (thus, it is larger), while the other particle exhibits a larger diffusion coefficient (thus, it is smaller) (Seinfeld and Pandis, 1998; Mönkkönen et al., 2004). Since fireworks emit extremely high concentrations (Table 1) of relatively large (d > 150 nm) particles into the air, they coagulate preferably with the smaller ambient particles. This is also confirmed by the time series of coagulation sink values (Fig. S9), which were very high for particles with d < 30 nm (mean $CoagS_6 = 1.4 \times 10^{-2}$ s^{-1} during the firework activity), and much smaller for d > 100 nm (mean $CoagS_{100} = 1.1 \times 10^{-4}$ s^{-1}).

The mean size distributions that were obtained by averaging the three most impacted individual spectra in each year (the spectra recorded at 21:29, 21:37 and 21:45 in 2021, Fig. 4) were fitted using lognormal functions and the resulted modal parameters are summarised in Table 1. The corresponding modal data for the years in which the smoke plume could not be identified are also given in Table 1 for completeness. The particle number size distributions in the ambient air in Budapest usually exhibit two modes. The Aitken mode shows a mean NMMD of 26 nm and the accumulation mode has a typical modal diameter of 93 nm (Salma et al., 2011a; Salma and Németh, 2019). The present parameters of the Aitken and accumulation modes are comparable to the values obtained earlier. It is mentioned for later comparison that the largest accumulation-mode diameters in Budapest were observed in the Castle District Tunnel (a microenvironment with the highest particle number concentrations as well). These diameters ranged up to 120 nm when the air ventilation of the tunnel was switched off (Salma et al., 2011b).

The mode associated with the firework activity is hereinafter referred to as firework mode. Its area varied in a wide range (by a factor of 24), thus the individual cases represented conditions with rather diverse firework source contributions and dispersion properties. The mean NMMD and SD were 203 ± 35 nm, which is larger than any other previously recorded modal diameter in Budapest. At the same time, this value agrees perfectly with the location of the firework-related mode reported in earlier studies, which was around 140 nm (Wehner et al., 2000), of 200–300 nm (Mönkkönen et al., 2004) and between 100 and 200 nm (Pirker et al., 2021).

High-temperature sources often emit relatively small particles (with NMMDs of 20–30 nm) (Raes et al., 2000). The modal diameters of firework particles are unusually large when considering the high temperatures of pyrotechnic deflagration of up to 2500 °C. However, the explosions take place in a dispersed manner in the air, i.e. far from being steady-state volumetric combustion conditions. This fact results in considerable T gradients and micrometeorological turbulent airflows around the fire spots. Most particles were likely generated in the adjacent zones with lower temperatures, which can explain the larger diameters. The equivalent diameters can also be influenced by

Table 1
Modal particle number concentrations (N_m in 10^3 cm^{-3}), particle number median mobility diameters (NMMD in nm) and geometric standard deviations (GSD) for the Aitken, accumulation and firework modes of the mean size distributions obtained by averaging the three most impacted individual spectra in 2016, 2017, 2021 and 2022. The modal parameters for 2014, 2015 and 2020, when there was no firework or the firework smoke could not be identified, were derived from the mean distributions obtained from three individual spectra between 21:00 and 21:30.

Year	Aitken mode			Accumulation mode			Firework mode		
	N_m	NMMD	GSD	N_m	NMMD	GSD	N_m	NMMD	GSD
2014	3.5	23	1.98	5.9	80	1.96	–		
2015	1.7	19	1.99	6.3	61	1.90	–		
2016	2.5	21	1.68	6.5	59	1.60	11.4	177	1.60
2017	1.6	20	1.68	4.8	49	1.77	4.9	168	1.71
2020	6.7	18	1.97	5.1	75	1.98	–		
2021	4.9	27	1.52	38	90	1.60	116	233	1.68
2022	1.3	21	1.60	18	90	1.76	100	232	1.68

transformation of the freshly emitted particles, which possess chain-like morphology transforming into more compact structures (Cao et al., 2018). The hygroscopic diameter growth of firework particles at larger values of RH – for instance above rivers – can also make the smoke thicker. The dense smoke of these particles is easily visible in the fading light of explosions and can even degrade visibility over extended air spaces. This is known to the providers of organised firework displays, and contributes to the fact that planned pauses are scheduled regularly in the course of such events (Fig. S6).

3.3. Residence times

The overall atmospheric residence time (τ, more precisely adjustment time) of the firework smoke particles was roughly estimated using the exponential decay curve analysis of atmospheric concentration. The details are given in Sect. S7. The resulting residence times were between 23 and 26 min in the denser smoke in 2017, 2021 and 2022, and it was approximately 1 h for the less concentrated smoke in 2016. The thicker plumes, which represent greater acute exposure to humans, can be fortunately characterised by shorter residence times.

The coagulation of the particles was identified as an important transformation process in the smoke. The partial atmospheric residence time for the coagulation of firework particles with a typical diameter of 200 nm with the pre-existing aerosol can be assessed as $\tau = 1/\mathrm{Coag}S_{200}$. These results were averaged for the time interval of the extended firework activity (21:00–22:00), and a typical value of 20 h was obtained. This is considerably larger than the overall residence time derived from the decay curve analysis. It means that removal processes other than coagulation must also contribute to this. These may include turbulent diffusion and condensational growth out of the measured diameter range. Evidence for the latter process comes from the elevated tail of the size distributions at the larger diameter end (Figs. 4 and S8) and from the very high CS during the display itself (Fig. S9). Such high CS values, with a mean of 0.74 s^{-1}, cause the condensable vapours to attach rapidly to the particles, which indirectly points to the significance of condensing vapours inside the smoke.

3.4. Atmospheric concentrations

The maxima of the hourly mean $N_{6–1000}$ and $N_{100–1000}$ in the firework plume in 2021 were 126 × 10^3 and 94 × 10^3 cm^{-3}, respectively, whereas the corresponding data for 2022 were 146 × 10^3 and 134 × 10^3 cm^{-3}. Similar concentrations were measured in Budapest only in polluted sub-local environments, such as road tunnels (Salma et al., 2011b, 2014). The weekly medians for the Castle District Tunnel in summer were 143 × 10^3 and 20 × 10^3 cm^{-3}, respectively. It has to be added that the chemical composition and thus, the health effects of these two types of particles can be rather different (Harrison, 2018; Harrison and Yin, 2000; Salma et al., 2002a; Moreno et al., 2007; Vecchi et al., 2008; Tanda et al., 2019). The concentration of some transition metals and heavy metals in the plume link these particles to their increased oxidative potential and health risk (Godri et al., 2010; Hickey et al., 2020).

The ratios r_{before} and r_{after} together with the values Z_{before} and Z_{after} (Eqs. (1) and (2)) are summarised in Table 2. In the most pronounced cases, i.e. in 2021 and 2022, the fireworks increased the hourly mean $N_{6–1000}$ by a mean factor and SD of 5.5 ± 0.7. The related differences were 13–23 times larger than the sample SD, which indicates the high reliability of the factors. The most sensitively affected 1-h concentration ($N_{100–1000}$) was increased by a mean factor and SD of 23 ± 3, and their related differences were 80–160 times higher than the sample SD. In the other two firework years (2016 and 2017), the r and values Z for the total particles were modest and ambiguous, but they were still evidently elevated for $N_{100–1000}$ (typically of 3 and 8, respectively). It should be noted that the effects of the fireworks on the measured concentrations were rather short in 2016 and 2017, which could be smoothed out by the adopted 1-h averaging time. The ratios for the different years could be also influenced by the absolute concentration levels, thus by the actual air quality just before the firework displays.

The contribution of ultrafine (UF) particles (d < 100 nm) to total particle numbers is often used to identify and characterise particle sources. Fossil fuel combustion, biomass burning and new particle formation and growth events usually increase the ambient UF-to-N_{6-1000} ratios. In contrast, the fireworks caused a substantial decrease from its urban level of 0.8–0.9 with a typical daily SD of 0.06 (Salma et al., 2014, 2021a) down to 0.2–0.3 as a consequence of the distinctive changes in the size distributions.

The effects of the fireworks in 2021 and 2022 on the PM mass were assessed from the particle number size distributions. The mean distributions of the three individual spectra before the fireworks (recorded at 20:58, 21:06 and 21:14 in 2021, Fig. 4), around their maximum influence (recorded at 21:29, 21:37 and 21:45) and after the size distribution reached the levels before the display (recorded at 22:25, 22:33 and 22:41), and hourly mean distributions before, during and well after the fireworks were considered. It is argued in Sect. S8 that the estimated PM mass corresponds to the PM_{10} size fraction with some larger uncertainties being possibly involved. However, the conversion was performed to approximate the PM mass elevation in a relative manner, and its results were interpreted in a comparative way, thus as mass ratios.

The fireworks in 2021 and 2022 at their peak influence increased the PM_{10} mass concentration at the BpART Lab by factors of 95 and 149, respectively for the ca. 25 min, relative to before or after the show. (The estimated peak concentrations in 2021 and 2022 were 4.1 and 3.6 mg m^{-3}, on adjoining background levels of 45 and 24 μg m^{-3}) These elevations were similar to those of 40-min displays at an international firework competition (Cao et al., 2018). The analogous ratios for the hourly mean size distributions were 41 and 74. These factors belong to the upper half of the increments observed in the world (Cao et al., 2018; Singh et al., 2019). It is noted that the measured PM_{10} mass concentrations with SDs averaged for the afternoons of interest in 2021 and 2022 were 21 ± 7 and 29 ± 11 μg m^{-3}, respectively at the nearest monitoring station of the National Air Quality Network in Budapest (at Széna Square) located upwind of the firework area.

Table 2
Concentration ratios (r) and values Z for the mean particle number concentrations during the firework event (21:00–22:00) with respect to the intervals before (20:00–21:00) and well after (22:30–23:30) the event in the size ranges from 6 to 1000 nm ($N_{6–1000}$) and from 100 to 1000 nm ($N_{100–1000}$) for all measurement years. In 2016, 2017, 2021 and 2022, the firework events were detected at the measurement site, in 2014 and 2015, the plume could not be detected, and in 2020 there were no fireworks.

Year	$N_{6–1000}$				$N_{100–1000}$			
	r_{before}	Z_{before}	r_{after}	Z_{after}	r_{before}	Z_{before}	r_{after}	Z_{after}
2014	1.2	0.63	0.75	−1.2	1.3	0.76	0.73	−1.1
2015	0.94	−0.20	1.3	0.65	1.2	1.6	1.2	1.4
2016	1.7	1.3	0.91	−0.34	2.8	7.7	1.6	5.2
2017	1.2	0.43	1.3	0.61	3.0	9.2	3.8	10
2020	1.1	0.34	0.92	−0.37	1.1	0.41	0.82	−1.2
2021	4.5	13	5.5	13	19	80	21	80
2022	5.8	23	6.1	23	25	161	26	161

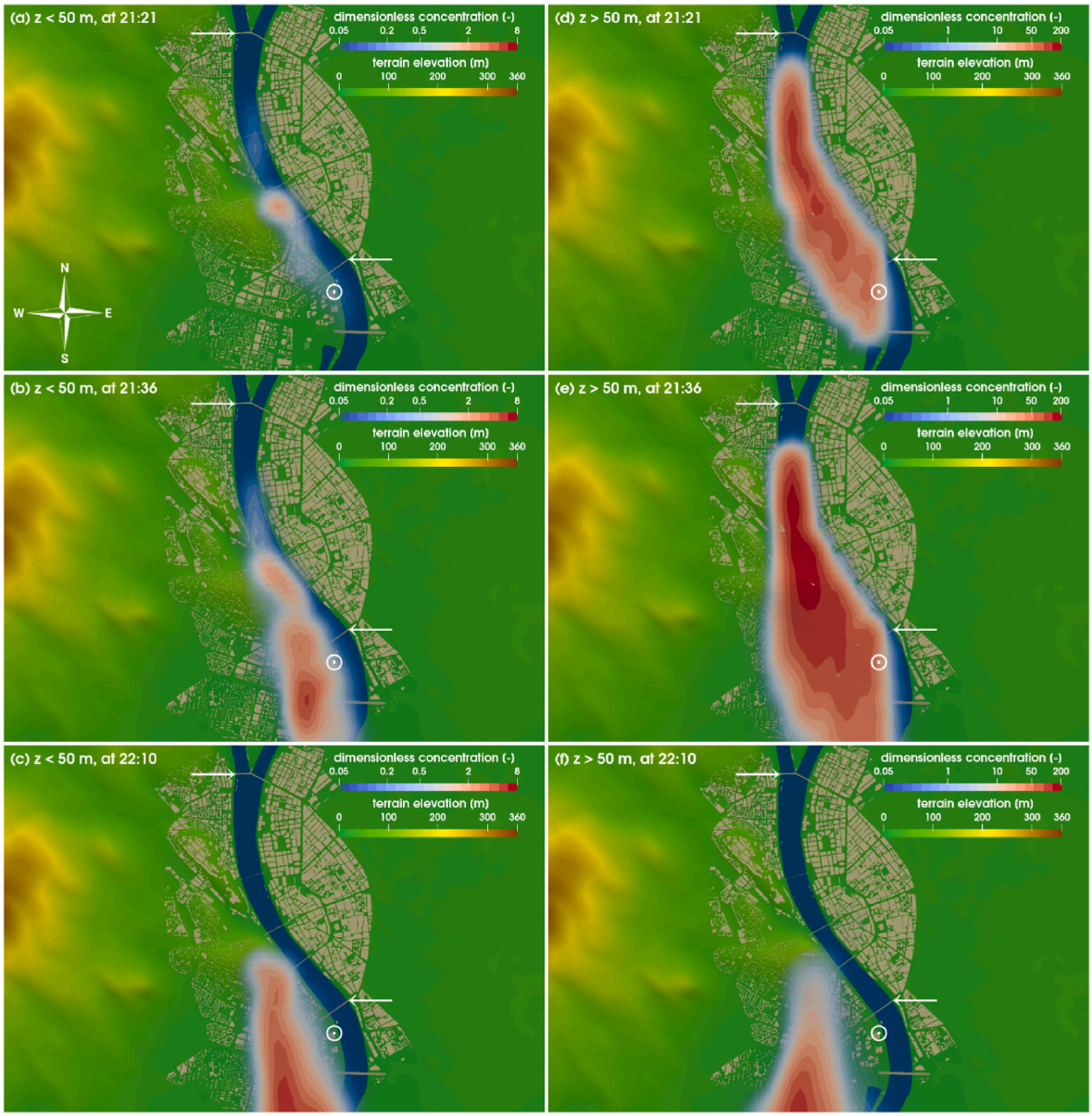

Fig. 5. Spatiotemporal dispersion of the firework smoke at the middle of the firework activity (21:21), at its maximum measured concentration (21:36) and after the return to the concentration levels before the show (22:10) in the near-surface layer ($z < 50$ m) and at greater heights ($z > 50$ m) on 20 August 2021. The bridges between which the firework displays took place above the Danube River are indicated by white arrows. The BpART Lab measurement site is marked with a white circle and dot.

3.5. Spatial extent and time development of the firework plumes

The modelled data for the measurement location in 2021 were normalised to the maximum measured value in order to compare the time evolution of the experimental and modelled data sets. The modelled curve followed the measured tendency reasonably well. The dispersions of the firework smoke in three different specifically selected times and in two vertical layers are shown in Fig. 5.

The results reveal that there were substantial vertical concentration gradients in the plume. The smoke above 50 m from the land surface ($z = 0$) (Fig. 5d–f) generally contained more particles (by a typical time-averaged mean factor of ca. 15) and also affected larger territories than the smoke below it (Fig. 5a–c). The overall area affected was mostly governed by the urban outflow and made up a very considerable portion of the city. The concentration differences in the plume in horizontal dimension were also large (by typical time-averaged mean factors of ca. 10 for the layer $z < 50$ m and of 60–100 for $z > 50$ m). Substantially higher concentrations were determined in the internal parts of the plume than near its boundaries. Fig. 5b also implies that the plume "edge" only touched the measurement site, so the real maximum atmospheric concentrations could be considerably higher than those dealt with in Sects. 3.1. and 3.4.

The dispersion modelling unambiguously demonstrates that not only the onsite spectators of the show and the people in closer adjacent environments, but inhabitants further away and more distant, large and populous urban quarters located downwind of the displays were also affected by the plume and its fallout.

3.6. Depositions in the respiratory system

The deposition fractions (probabilities) for the case of a female in 2021 exhibited a shape which depended basically on particle number size distribution (Fig. S2). As a consequence, the curves for the cases before and after the fireworks were similar. The distribution of maximum firework influence was placed substantially lower and the location of this maximum was shifted to larger airway generation numbers compared to the cases before and after the displays. The shift in the generation number was caused by the increase in the median particle diameter. The lowering in peak height may be explained by the fact that deposition probability decreases with particle diameter in this diameter region (e.g. Fig. 2 in Salma et al., 2015). Approximately half (55%) of the inhaled particles were exhaled before and after the fireworks, whereas this was higher (77%) during peak firework influence. For the case of a child, the situation was qualitatively similar and 86% of the inhaled particles were exhaled. This was caused by the differences in the physiological respiratory parameters and morphometric data for children and adults (Sect. S4).

The fireworks substantially changed the atmospheric concentrations as well. Their actual values in the plume at the receptor site before, during and after the firework influence in 2021 were derived from the corresponding mean size distributions as 22×10^3, 156×10^3 and 17×10^3 cm^{-3}, respectively. Deposition rates were computed taking these values into account (Fig. S3). The curve for the maximum influence stood out conspicuously from the other two lines, which indicates extraordinarily intensive deposition. The deposition rate for the case of a child appeared smaller in amplitude, but its maximum was shifted to smaller generation numbers similarly to that for a female.

The differences among the curves for the case of a female were quantified by integrating the deposition rates over the main anatomical regions (Table S2). The derived values were very high, in the order of 10^7–10^8 min^{-1}, and correspond to urban microenvironments with extremely high pollution levels (Kumar et al., 2012). The smallest and the largest deposition rates occurred uniformly in the conductive airways (TB tree) and in the AC region, respectively. The fireworks increased the deposition rate in the whole respiratory system by a factor of 4. The increments were primarily governed by atmospheric concentrations. The elevation in the total deposition rate (by 4) was, however, smaller than that of atmospheric concentration (by 5 for 1-h means). This difference was caused by alterations in the size distributions.

In contrast to the deposition fractions and deposition rates, the surface density deposition rates exhibited a very different shape with the highest surface loading being in the second and third airway generations (segmental and sub-segmental bronchi; Fig. 6). This can be explained by the fact that the epithelial surface area is the smallest for the airway generations of 2–4. Since children have smaller airways with a much smaller surface area, their surface density deposition rates were higher than in adults. Furthermore, the maximum of this deposition rate during the highest firework influence was shifted to the trachea (airway generation 1), and this was increased with respect to a female even more than in the segmental bronchi. These results together suggest that children are more susceptible to particle exposure from fireworks than adults, despite the fact that their deposition fractions were smaller than for adults.

4. Conclusions

The results and conclusions obtained are generally and qualitatively valid for many firework displays around the world and contribute to better understanding of the phenomenon. It is estimated that several hundred million people are exposed to high concentrations of smoke originating from fireworks.

The benefits and attraction of firework displays are generally known. Here we mainly focused on and quantified several pieces of scientific evidence of the hazards and risk of fireworks. The continuation of cultural traditions and the enjoyment related to firework displays on the one hand, and the complex, potentially adverse health and environmental effects on the other hand must be judged together. It should also be recognised that the emissions from energy production, such as electricity generation, heating, transport and from agriculture are mostly related to serving basic human and societal needs, while firework displays are often organised only for pleasure. Because of the impacts documented here, fireworks as pollution for pleasure need to be regulated and replaced with other forms of entertainment. Eventually, it is up to the local communities involved to decide in a balanced manner whether this form of amusement is worth the risky atmospheric cocktail it generates.

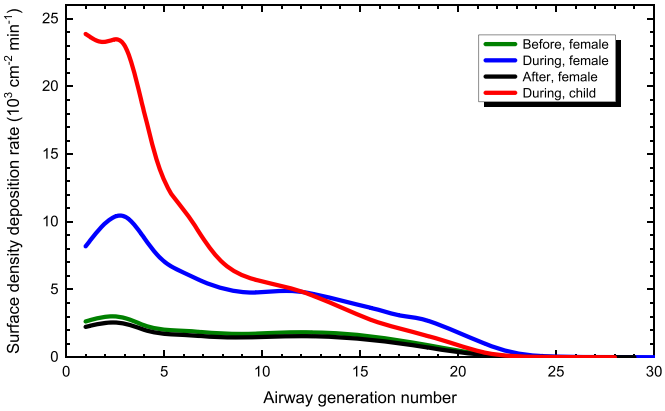

Fig. 6. Surface density deposition rates of aerosol particles in the airway generations of an adult female performing reference seated physical activity before the firework influence (with a particle number concentration of 22×10^3 cm^{-3} measured by the DMPS system), during (156×10^3 cm^{-3}) and after it (17×10^3 cm^{-3}) in 2021. The corresponding distribution for a 5-year-old child during the firework is also added.

Declaration of competing interest

The authors declare that they have no known competing financial interests or personal relationships that could have appeared to influence the work reported in this paper.

Data availability

Data will be made available on request.

Acknowledgements

Funding by the Hungarian Research, Development and Innovation Office (K132254 and K124439) is acknowledged. The research carried out at Budapest University of Technology and Economics is part of the project TKP-6-6/PALY-2021, implemented with the support provided by the Ministry of Culture and Innovation of Hungary from the National Research, Development and Innovation Fund, financed under the TKP2021-NVA funding scheme. The authors are grateful to Ferenc Tóth, director of Nuvu Ltd., Budapest for the detailed data on the firework display in 2021, to András Zénó Gyöngyösi of Eötvös Loránd University for the aerosol measurements and to Péter Füri of Centre for Energy Research for his help in the respiratory system deposition calculations.

Credit author statement

I. Salma: Conceptualization, Methodology, Investigation, Visualization, Supervision, Writing - original draft, Funding acquisition; Á. Farkas: Methodology, Investigation, Software, Writing - review & editing; T. Weidinger: Validation, Methodology, Investigation, Writing - review & editing; M. Balogh: Methodology, Investigation, Software, Visualization, Writing – review & editing, Funding acquisition.

Appendix A. Supplementary data

Supplementary data to this article can be found online at https://doi.org/10.1016/j.envpol.2023.121612.

References

Bach, W., Daniels, A., Dickinson, L., Hertlein, F., Morrow, J., Margolis, S., Dinh, V., 2007. Fireworks pollution and health. Pol. J. Environ. Stud. 7, 183–192. https://doi.org/10.1080/00207237508709692.

Balásházy, I., Alföldy, B., Molnár, A.J., Hofmann, W., Szőke, I., Kis, E., 2007. Aerosol drug delivery optimization by computational methods for the characterization of total and regional deposition of therapeutic aerosols in the respiratory system. Curr. Comput. Aided Drug Des. 3, 13–32. https://doi.org/10.2174/157340907780058727.

Balogh, M., Parente, A., Benocci, C., 2012. RANS simulation of ABL flow over complex terrains applying an enhanced k-epsilon model and wall function formulation: implementation and comparison for Fluent and OpenFOAM. J. Wind Eng. Ind. Aerod. 104 (106), 360–368. https://doi.org/10.1016/j.jweia.2012.02.023.

Balogh, M., Parente, A., 2015. Realistic boundary conditions for the simulation of atmospheric boundary layer flows using an improved k–ε model. J. Wind Eng. Ind. Aerod. 144, 183–190. https://doi.org/10.1016/j.jweia.2015.01.010.

Baranyai, E., Simon, E., Braun, M., Tóthmérész, B., Posta, J., Fábián, I., 2014. The effect of a fireworks event on the amount and elemental concentration of deposited dust collected in the city of Debrecen, Hungary. Air Qual. Atmos. Health 8, 359–365. https://doi.org/10.1007/s11869-014-0290-7.

Barman, S.C., Singh, R., Negi, M.P., Bhargava, S.K., 2008. Ambient air quality of Lucknow City (India) during use of fireworks on Diwali festival. Environ. Monit. Assess. 137, 495–504. https://doi.org/10.1007/s10661-007-9784-1.

Cao, X., Zhang, X., Tong, D.Q., Chen, W., Zhang, S., Zhao, H., Xiu, A., 2018. Review on physicochemical properties of pollutants released from fireworks: environmental and health effects and prevention. Environ. Rev. 26, 133–155. https://doi.org/10.1139/er-2017-0063.

Dickerson, A.S., Benson, A.F., Buckley, B., Chan, E.A.W., 2017. Concentrations of individual fine particulate matter components in the USA around July 4th. Air Qual. Atmos. Health 10, 349–358. https://doi.org/10.1007/s11869-016-0433-0.

Drewnick, F., Hings, S.S., Curtius, J., Eerdekens, G., Williams, J., 2006. Measurement of fine particulate and gas-phase species during the New Year's fireworks 2005 in Mainz, Germany. Atmos. Environ. Times 40, 4316–4327. https://doi.org/10.1016/j.atmosenv.2006.03.040.

Duna Media Service Provider, 2022. in Hungarian, last downloaded. https://dunamsz.hu/2022/08/30/rekordnezettseget-hozott-a-tuzijatek. (Accessed 15 February 2023).

Farkas, Á., Füri, P., Thén, W., Salma, I., 2022. Effects of hygroscopic growth of urban aerosol particles on their modelled regional and local deposition in healthy and COPD-compromised human respiratory system. Sci. Total Environ. 806, 151202 https://doi.org/10.1016/j.scitotenv.2021.151202.

Fu, H., Yang, Z., Liu, Y., Shao, P., 2021. Ecological and human health risk assessment of heavy metals in dust affected by fireworks during the Spring Festival in Beijing. Air Qual. Atmos. Health. 14, 139–148. https://doi.org/10.1007/s11869-020-00920-9.

Godri, K.J., Green, D.C., Fuller, G.W., Dall'Osto, M., Beddows, D.C., Kelly, F.J., Harrison, R.M., Mudway, I.S., 2010. Particulate oxidative burden associated with firework activity. Environ. Sci. Technol. 44, 8295–8301. https://doi.org/10.1021/es1016284.

Greven, F.E., Vonk, J.M., Fischer, P., Duijm, F., Vink, N.M., Brunekreef, B., 2019. Air pollution during New Year's fireworks and daily mortality in The Netherlands. Sci. Rep. 9, 5735. https://doi.org/10.1038/s41598-019-42080-6.

Harrison, R.M., 2018. Urban atmospheric chemistry: a very special case for study. Clim. Atmos. Sci. 1, 20175 https://doi.org/10.1038/s41612-017-0010-8.

Harrison, R.M., Yin, J., 2000. Particulate matter in the atmosphere: which particle properties are important for its effects on health? Sci. Total Environ. 249, 85–101. https://doi.org/10.1016/S0048-9697(99)00513-6.

Hickey, C., Gordon, C., Galdanes, K., Blaustein, M., Horton, L., Chillrud, S., Ross, J., Yinon, L., Chen, L. Ch, Gordon, T., 2020. Toxicity of particles emitted by fireworks. Part. Fiber Toxicol. 17, 28. https://doi.org/10.1186/s12989-020-00360-4.

Hofmann, W., 2011. Modelling inhaled particle deposition in the human lung – a review. J. Aerosol Sci. 42, 693–724. https://doi.org/10.1016/j.jaerosci.2011.05.007.

Holmes, N.S., Morawska, L., 2006. A review of dispersion modelling and its application to the dispersion of particles: an overview of different dispersion models available. Atmos. Environ. 40, 5902–5928. https://doi.org/10.1016/j.atmosenv.2006.06.003.

Hussein, T., Puustinen, A., Aalto, P.P., Mäkelä, J.M., Hämeri, K., Kulmala, M., 2004. Urban aerosol number size distributions. Atmos. Chem. Phys. 4, 391–411. https://doi.org/10.5194/acp-4-391-2004.

Jiang, Q., Sun, Y.L., Wang, Z., Yin, Y., 2015. Aerosol composition and sources during the Chinese Spring Festival: fireworks, secondary aerosol, and holiday effects. Atmos. Chem. Phys. 15, 6023–6034. https://doi.org/10.5194/acp-15-6023-2015.

Joly, A., Smargiassi, A., Kosatsky, T., Fournier, M., Zlotorzynska, D.E., Celo, V., Mathieu, D., Servranckx, R., D'amours, R., Malo, A., Brook, J., 2010. Characterization of particulate exposure during fireworks displays. Atmos. Environ. 44, 4325–4329. https://doi.org/10.1016/j.atmosenv. 2009.12.010.

Kulmala, M., Dal Maso, M., Mäkelä, J.M., Pirjola, L., Väkevä, M., Aalto, P., Miikkulainen, P., Hämeri, K., O'Dowd, C.D., 2001. On the formation, growth and composition of nucleation mode particles. Tellus B 53, 479–490. https://doi.org/10.1034/j.1600-0889.2001.530411.x.

Kulmala, M., Petäjä, T., Nieminen, T., Sipilä, M., Manninen, H.E., Lehtipalo, K., Dal Maso, M., Aalto, P.P., Junninen, H., Paasonen, P., Riipinen, I., Lehtinen, K.E.J., Laaksonen, A., Kerminen, V.-M., 2012. Measurement of the nucleation of atmospheric aerosol particles. Nat. Protoc. 7, 1651–1667. https://doi.org/10.1038/nprot.2012.091.

Kumar, P., Morawska, L., Harrison, R.M., 2012. Nanoparticles in European cities and associated health impacts. In: Amato, F., et al. (Eds.), Urban Air Quality in Europe, The Handbook of Environmental Chemistry, vol. 26. Springer, Berlin, pp. 339–365. https://doi.org/10.1007/698_2012_161.

Kumar, P., Morawska, L., Birmili, W., Paasonen, P., Hu, M., Kulmala, M., Harrison, R.M., Norford, L., Britter, R., 2014. Ultrafine particles in cities. Environ. Int. 66, 1–10. https://doi.org/10.1016/j.envint.2014.01.013.

Lin, Ch-Ch, 2016. A review of the impact of fireworks on particulate matter in ambient air. J. Air Waste Manage. Assoc. 66, 1171–1182. https://doi.org/10.1016/10.1080/10962247.2016.1219280.

Mikkonen, S., Németh, Z., Varga, V., Weidinger, T., Leinonen, V., Yli-Juuti, T., Salma, I., 2020. Decennial time trends and diurnal patterns of particle number concentrations in a central European city between 2008 and 2018. Atmos. Chem. Phys. 20, 12247–12263. https://doi.org/10.5194/acp-20-12247-2020.

Moreno, T., Querol, X., Alastuey, A., Minguillòn, M.C., Pey, J., Rodriguez, S., Mirò, J.V., Felis, C., Gibbons, W., 2007. Recreational atmospheric pollution episodes: inhalable metalliferous particles from firework displays. Atmos. Environ. 41, 913–922. https://doi.org/10.1016/j.atmosenv.2006.09.019.

Moreno, T., Querol, X., Alastuey, A., Amato, F., Pey, J., Pandolfi, M., Kuenzli, N., Bouso, L., Rivera, M., Gibbons, W., 2010. Effect of fireworks events on urban background trace metal aerosol concentrations: is the cocktail worth the show? J. Hazard Mater. 183, 945–949. https://doi.org/10.1016/j.jhazmat.2010.07.082.

Mousavi, A., Yuan, Y., Masri, S., Barta, G., Wu, J., 2021. Impact of 4th of July fireworks on spatiotemporal $PM_{2.5}$ concentrations in California based on the PurpleAir Sensor Network: implications for policy and environmental justice. Int. J. Environ. Res. Publ. Health 18, 5735. https://doi.org/10.3390/ijerph18115735.

Mönkkönen, P., Koponen, I.K., Lehtinen, K.E.J., Uma, R., Srinivasan, D., Hämeri, K., Kulmala, M., 2004. Death of nucleation and Aitken mode particles: observations at extreme atmospheric conditions and their theoretical explanation. J. Aerosol Sci. 35, 781–787. https://doi.org/10.1016/j.jaerosci.2003.12.004.

Pirker, L., Velkavrh, Ž., Osïte, A., Drinovec, L., Močnik, G., Remškar, M., 2021. Fireworks – a source of nanoparticles, PM2.5, PM10, and carbonaceous aerosols. Air Qual. Atmos. Health. https://doi.org/10.1007/s11869-021-01142-3.

Raes, F., Van Dingenen, R., Vignati, E., Wilson, J., Putaud, J., Seinfeld, J., Adams, P., 2000. Formation and cycling of aerosols in the global troposphere. Atmos. Environ. Times 34, 4215–4240. https://doi.org/10.1016/S1352-2310(00)00239-9.

Salma, I., Maenhaut, W., Záray, Gy, 2002a. Comparative study of elemental mass size distributions in urban atmospheric aerosol. J. Aerosol Sci. 33, 339–356. https://doi.org/10.1016/S0021-8502(01)00176-8.

Salma, I., Balásházy, I., Hofmann, W., Záray, Gy, 2002b. Effect of physical exertion on the deposition of urban aerosols in the human respiratory system. J. Aerosol Sci. 33, 983–997. https://doi.org/10.1016/S0021-8502(02)00051-4.

Salma, I., Borsós, T., Weidinger, T., Aalto, P., Hussein, T., Dal Maso, M., Kulmala, M., 2011a. Production, growth and properties of ultrafine atmospheric aerosol particles in an urban environment. Atmos. Chem. Phys. 11, 1339–1353. https://doi.org/10.5194/acp-11-1339-2011.

Salma, I., Borsós, T., Aalto, P.P., Kulmala, M., 2011b. Time-resolved number concentration and size distribution of aerosol particles in an urban road tunnel. Boreal Environ. Res. 16, 262–272.

Salma, I., Borsós, T., Németh, Z., Weidinger, T., Aalto, T., Kulmala, M., 2014. Comparative study of ultrafine atmospheric aerosol within a city. Atmos. Environ. 92, 154–161. https://doi.org/10.1016/j.atmosenv.2014.04.020.

Salma, I., Füri, P., Németh, Z., Farkas, Á., Balásházy, I., Hofmann, W., Farkas, Á., 2015. Lung burden and deposition distribution of inhaled atmospheric urban ultrafine particles as the first step in their health risk assessment. Atmos. Environ. Times 104, 39–49. https://doi.org/10.1016/j.atmosenv.2014.12.060.

Salma, I., Németh, Z., Weidinger, T., Kovács, B., Kristóf, G., 2016. Measurement, growth types and shrinkage of newly formed aerosol particles at an urban research platform. Atmos. Chem. Phys. 16, 7837–7851. https://doi.org/10.5194/acp-16-7837-2016.

Salma, I., Németh, Z., 2019. Dynamic and timing properties of new aerosol particle formation and consecutive growth events. Atmos. Chem. Phys. 19, 5835–5852. https://doi.org/10.5194/acp-19-5835-2019.

Salma, I., Thén, W., Aalto, P., Kerminen, V.-M., Kern, A., Barcza, Z., Petäjä, T., Kulmala, M., 2021a. Influence of vegetation on occurrence and time distributions of regional new aerosol particle formation and growth. Atmos. Chem. Phys. 21, 2861–2880. https://doi.org/10.5194/acp-21-2861-2021.

Salma, I., Thén, W., Vörösmarty, M., Gyöngyösi, A.Z., 2021b. Cloud activation properties of aerosol particles in a continental Central European urban environment. Atmos. Chem. Phys. 21, 11289–11302. https://doi.org/10.5194/acp-21-11289-2021.

Sarkar, S., Khillare, P.S., Jyethi, D.S., Hasan, A., Parween, M., 2010. Chemical speciation of respirable suspended particulate matter during a major firework festival in India. J. Hazard Mater. 184, 321–330. https://doi.org/10.1016/j.jhazmat.2010.08.039.

Seidel, D.J., Birnbaum, A.N., 2015. Effects of Independence Day fireworks on atmospheric concentrations of fine particulate matter in the United States. Atmos. Environ. 115, 192–198. https://doi.org/10.1016/j.atmosenv.2015.05.065.

Seinfeld, J.H., Pandis, S.N., 1998. Atmospheric Chemistry and Physics: from Air Pollution to Climate Change. Wiley, Hoboken, USA.

Sijimol, M.R., Mohan, M., 2014. Environmental impacts of perchlorate with special reference to fireworks – a review. Environ. Monit. Assess. 186, 7203–7210. https://doi.org/10.1007/s10661-014-3921-4.

Singh, A., Pant, P., Pope, F.D., 2019. Air quality during and after festivals: aerosol concentrations, composition and health effects. Atmos. Res. 227, 220–232. https://doi.org/10.1016/j.atmosres.2019.05.012.

Sun, Y., Han, Z., Du, Z., Li, Z., Cong, X., 2017. Preparation and performance of environmental friendly sulphur-free propellant for fireworks. Appl. Therm. Eng. 126, 987–996. https://doi.org/10.1016/j.applthermaleng.2017.08.003.

Tanda, S., Ličbinský, R., Hegrová, J., Goessler, W., 2019. Impact of New Year's Eve fireworks on the size resolved element distributions in airborne particles. Environ. Int. 128, 371–378. https://doi.org/10.1016/j.envint.2019.04.071.

Vecchi, R., Bernardoni, V., Cricchio, D., D'Alessandro, A., Fermo, P., Lucarelli, F., Nava, S., Piazzalunga, A., Valli, G., 2008. The impact of fireworks on airborne particles. Atmos. Environ. 42, 1121–1132. https://doi.org/10.1016/j.atmosenv.2007.10.047.

Wehner, B., Wiedensohler, A., Heintzenberg, J., 2000. Submicrometer aerosol size distributions and mass concentration of the Millennium fireworks 2000 in Leipzig, Germany. J. Aerosol Sci. 31, 1489–1493. https://doi.org/10.1016/S0021-8502(00)00039-2.

Wiedensohler, A., Birmili, W., Nowak, A., Sonntag, A., Weinhold, K., Merkel, M., Wehner, B., Tuch, T., Pfeifer, S., Fiebig, M., Fjäraa, A.M., Asmi, E., Sellegri, K., Depuy, R., Venzac, H., Villani, P., Laj, P., Aalto, P., Ogren, J.A., Swietlicki, E., Williams, P., Roldin, P., Quincey, P., Hüglin, C., Fierz-Schmidhauser, R., Gysel, M., Weingartner, E., Riccobono, F., Santos, S., Grüning, C., Faloon, K., Beddows, D., Harrison, R., Monahan, C., Jennings, S.G., O'Dowd, C.D., Marinoni, A., Horn, H.-G., Keck, L., Jiang, J., Scheckman, J., McMurry, P.H., Deng, Z., Zhao, C.S., Moerman, M., Henzing, B., de Leeuw, G., Löschau, G., Bastian, S., 2012. Mobility particle size spectrometers: harmonization of technical standards and data structure to facilitate high quality long-term observations of atmospheric particle number size distributions. Atmos. Meas. Tech. 5, 657–685. https://doi.org/10.5194/amt-5-657-2012.

Yang, S., Li, P., Liu, J., Bi, X., Ning, Y., Wang, S., Wang, P., 2019. Profiles, source identification and health risks of potentially toxic metals in pyrotechnic-related road dust during Chinese New Year. Ecotoxicol. Environ. Saf. 184, 109604 https://doi.org/10.1016/j.ecoenv.2019.109604.

Zhang, J., Lance, S., Freedman, J.M., Sun, Y., Crandall, B.A., Wei, X., Schwab, J.J., 2019. Detailed measurements of submicron particles from an Independence Day fireworks event in Albany, New York using HR-ToF-AMS. Earth Space Chem 3, 1451–1459. https://doi.org/10.1021/acsearthspacechem.9b00046.

Zhang, M., Wang, X., Chen, J., Cheng, T., Wang, T., Yang, X., Gong, Y., Geng, F., Chen, Ch, 2010. Physical characterization of aerosol particles during the Chinese New Year's firework events. Atmos. Environ. 44, 5191–5198. https://doi.org/10.1016/j.atmosenv.2010.08.048.

Supplementary Material to:
Firework smoke: impacts on urban air quality and deposition in the human respiratory system

Imre Salma[a,*], Árpád Farkas[b], Tamás Weidinger[c], Miklós Balogh[d]

[a] *Institute of Chemistry, Eötvös Loránd University, Budapest, Hungary*
[b] *Center for Energy Research, Budapest, Hungary*
[c] *Department of Meteorology, Institute of Geography and Earth Sciences, Eötvös Loránd University, Budapest, Hungary*
[d] *Department of Fluid Mechanics, Faculty of Mechanical Engineering, Budapest University of Technology and Economics, Budapest, Hungary*

S1. Fireworks and their effects

Fireworks are small pyrotechnic devices that explode in the air and create bursts of brightly coloured light and sudden, loud sound effects. They contain: 1) propellant and fuel, 2) oxidants and 3) metals, whose electron excitation at the high temperatures of deflagration yields the coloured displays (Russell, 2009; Sun et al., 2017; Cao et al., 2018). The first group conventionally contains C (in forms of carbon black, sugar or starch), elemental S and P, and possibly some fuel metals such as Mg, Al, Fe and Zn. The oxidants are made of nitrates, perchlorate, chlorates or hydrogen terephthalate salts (of K), which support the combustion of the fuel. The last group of ingredients includes Li, Na, Al, Ca, Ti, Fe, Co, Cu, Zn, Sr, Ba and Pb compounds (Russell, 2009; Hickey et al., 2020). They generate an assortment of colours, for instance, Sr red, Ba green, Cu blue, Ca orange, Li pink and Na yellow (Lin, 2016). Sometimes the same substance is used to provide both colour and oxygen or for stabilising the mixture. Additional compounds are added for specific functions, such as organic dyes for smoke generation, Ti to enhance the production of sparks, metal salicylates for noise effects and chlorinated organics for colour enhancement or deepening.

Compared to ordinary levels, firework displays increased the particulate matter (PM) mass in various size fractions by a typical factor of 2–6 considering longer-time (24-h) means, or even by much more for shorter terms (Joly et al., 2010; Seidel and Birnbaum, 2015; Lin, 2016; Cao et al., 2018 and references therein; Greven at al., 2019; Singh et al., 2019 and references therein; Mousavi et al., 2021; Pirker et al., 2021). The amounts of several constituents such as metals,

* Corresponding author.
E-mail address: salma.imre@ttk.elte.hu (I. Salma).

Cl, P and some polyaromatic hydrocarbons (PAHs) in the smoke were often much higher than this increment by a factor of up to 10^2 (Moreno et al., 2007, 2010; Barman et al., 2008; Vecchi et al., 2008; Sarkar et al., 2010; Lin, 2016; Dickerson et al., 2017; Cao et al., 2018; Tanda et al., 2019). Atmospheric concentrations strongly depend on local conditions, such as the distance of the receptor site from the source, meteorological and orogenic factors and the actual firework activity. The concentrations of metals in PM mass can be more demonstrative of the actual pollutants involved: Al 9%, Ti 2%, Fe 0.6%, Co 0.02%, Cu 5%, Zn 0.2%, Sr 0.6%, Ba 1%, and Pb 4% (Hickey et al., 2020), with these concentrations mainly depending on the type of firework used.

The biochemical effects of firework particles are related mainly to mass metrics, such as the mass of PM or metals. Size-fractionated aerosol samples from fireworks were collected in a steel chamber and were evaluated for their toxicity in cells and in vivo in mice treated by oropharyngeal aspiration (Hickey et al., 2020). At doses that did not produce cytotoxicity, in vitro reactive oxygen species (ROS) formation was measured in bronchial epithelial airways and human pulmonary microvascular endothelial cell lines treated with particles from the firework emissions. Significant increases in ROS in both cell types depended on the metal contents but not on particle size. The in vitro ROS activity significantly correlated with lung inflammation produced in mice. The findings showed that firework particles can produce severe adverse effects in mammalian cells and lungs.

The biological responses in humans (e.g. Harrison and Yin, 2000) are expected to be mainly manifested as the acute health effects evoked by the inhalation of smoke (Godri et al., 2010). The similarities and differences between short-term and long-term exposures were investigated in dedicated studies (Schwartz et al., 2008; Shi et al., 2016). The acute exposures of healthy young individuals are better tolerated than chronic exposures (Gao et al., 2021). The former can cause coughing, dyspnoea and fever (Hirai et al., 2000). Short-term $PM_{2.5}$ exposures were also associated with the exacerbation of illness in people with a respiratory disease, such as asthma and chronic obstructive pulmonary disease, and with an increase in the number of deaths from cardiovascular, respiratory and cerebrovascular diseases among the elderly (Orellano et al., 2020). Such exposure can lead to cognitive decline (Shehab and Pope, 2019), problems with heart rate and its variability, especially in obese individuals (Li et al., 2021). There is scientific evidence that short-term exposure to $PM_{2.5}$ mass is associated with attention deficit in adolescence (Park et al., 2020), worsening lung function in children (Hoek et al., 1998; Tasmin et al., 2019) and exposure within one day before the onset of ischemic stroke is linked to the

subsequent occurrence of ischemic stroke (Matsuo et al., 2016). Heavy and transition metals, and PAHs in PM can greatly contribute to and can raise both cancer and non-carcinogenic risk (Burki, 2017; Harrison et al., 2017).

The flashes and sound from the explosions can trigger psychological stress and can cause ocular and hearing trauma. In addition, the blasts can frighten animals, including household pets. Physical, even fatal injury can occur due to explosions in firework factories and stores, as well due to consumer use of commercially available firework kits and firecrackers (Cao et al., 2018). All these concerns have led to stricter controls on the licenced sale of fireworks and on discharge time intervals, and to the regulation of municipal firework displays in some large cities (Cao et al., 2018; Yao et al., 2019; Mousavi et al., 2021).

S2. Details of the studied displays

The firework displays on 20 August are organised to celebrate the national holiday in commemoration of the foundation of the state of Hungary. The launching devices in Budapest are deployed from boats and bridges. The source area is defined by the rectangular area bordered by the bridges over the Danube and the riverbank (Table S1). The largest longitudinal extension of the source area is approximately 4.3 km. The shortest and the longest distances between the measurement location (BpART Lab) and the source area in the most impacted years were approximately 400 m and 5 km. The firework displays have been gradually extended and developed to include complex artistic audiovisual elements, including music, narratives, dialogues and smart illumination of buildings and using drones.

Table S1. The number of fireworks, the bordering bridges of the source area complementing Fig. 1, the source area of the fireworks together with indication of the availability of the measured aerosol data on 20 August for the years 2014–2022. The firework display in 2022 was postponed from 20 to 27 of August.

Year	No. of effects (10^3)	Bordering bridges (north, south)	Source area (km^2)	Data available
2014	11	Margaret, Petőfi	1.8	yes
2015	10	Széchenyi, Liberty	0.50	yes
2016	21	Széchenyi, Elisabeth	0.31	yes
2017	25	Margaret, Széchenyi	0.62	yes
2018	21	Margaret, Elisabeth	1.0	no
2019	26	Széchenyi, Elisabeth	0.31	no
2020	no fireworks	–	–	yes
2021	33	Margaret, Petőfi	1.8	yes
2022	40	Margaret, Petőfi	1.8	yes

S3. Details of the dispersion modelling

The dispersion of the firework smoke was assessed with the primary purpose of getting an idea of the spatiotemporal development of and the relative unevenness within the particle plume. The numerical simulations were carried out using the open-source CFD toolbox OpenFOAM.

The domain geometry was reconstructed from various geographic information system (GIS) datasets. The main source was the CORINE Land Cover (CLC) inventory (Bossard et al., 2000), specifically its Urban Atlas database (Copernicus Land Monitoring, 2018a). This provides pan-European comparable land cover and land use data for functional urban areas. It was obtained from the Copernicus Land Monitoring Service, and it consists of an inventory of land cover in 44 classes (Copernicus Land Monitoring, 2018b). In this study, CLC2018 was used during computer-aided design (CAD) to derive the important surface coverage parameters. Surface roughness based on CORINE data was successfully used in several earlier atmospheric studies (e.g. Hasager et al., 2003; Silva et al., 2007; De Meij, 2014; Jancewicz, 2014). In the present work, a roughness classification similar to Silva et al. (2007) was adopted in the fully implicit regions due to its completeness and applicability. In order to convert the GIS data to the Cartesian coordinate system, its WGS84 geographical coordinates were reprojected to the Cartesian system using conformal cylindrical projection (Uniform National Projection system). This is generally used for regional GIS applications in Hungary.

The built environment in the internal part of the domain requires building data, which were obtained from the OpenStreetMap (OSM) database (OpenStreetMap Foundation, 2021). The terrain elevation data were derived from the Shuttle Radar Topography Mission (SRTM 1A) database, which offers worldwide coverage with a typical resolution of 30 m. Urban forest density also originated from the CLC2018 database, but the forest height was obtained from the Global Land Analysis and Discovery database (Potapov et al., 2020).

According to a proven methodology (Balogh and Kristóf, 2010), the domain was constructed from concentric regions using the formerly introduced datasets. In order to simplify the specification of the boundary conditions, some modifications connected to the lateral boundaries had to be applied on the outer regions. Both the elevation and surface coverage data were relaxed in space to their reference values along the relaxation zone from the edge of the examination area towards the lateral boundaries. The reference value for elevation was its spatial minimum in the domain area, whereas for the specification of the relaxed surface coverage parameters, the properties of the suburban area were used as the reference. In this way, identical vertical profiles could be imposed at the lateral sides of the domain. The

dimensions of the domain were 16×16×4 km, including a well detailed circular inner region with a diameter of 6.4 km in the city centre. The relaxation zone was ring shaped around the examination area (with a diameter of 9.6–14 km). In the examination area, most of the suitable (larger) OSM buildings were created virtually. Urban Atlas building height raster data were used to supplement missing building heights. The pre-processed GIS data were utilised to create the CAD geometry of the entire domain (Fig. S1a).

The CAD geometry of the complex urban texture of the studied area (Fig. 1) was finally discretised using a high-resolution computational mesh (Fig. S1b). The minimum cell size was between 2 and 4 m at the bridges and nearby building edges, and this gradually increased to 16–32 m in the inner region of the domain (examination area). Far from the ground surface and from the examination area, cell size was maximized at 128 m. The mesh resolution determined the feature size in the different regions. The total number of cells in the mesh was ca. 3.6×10^7.

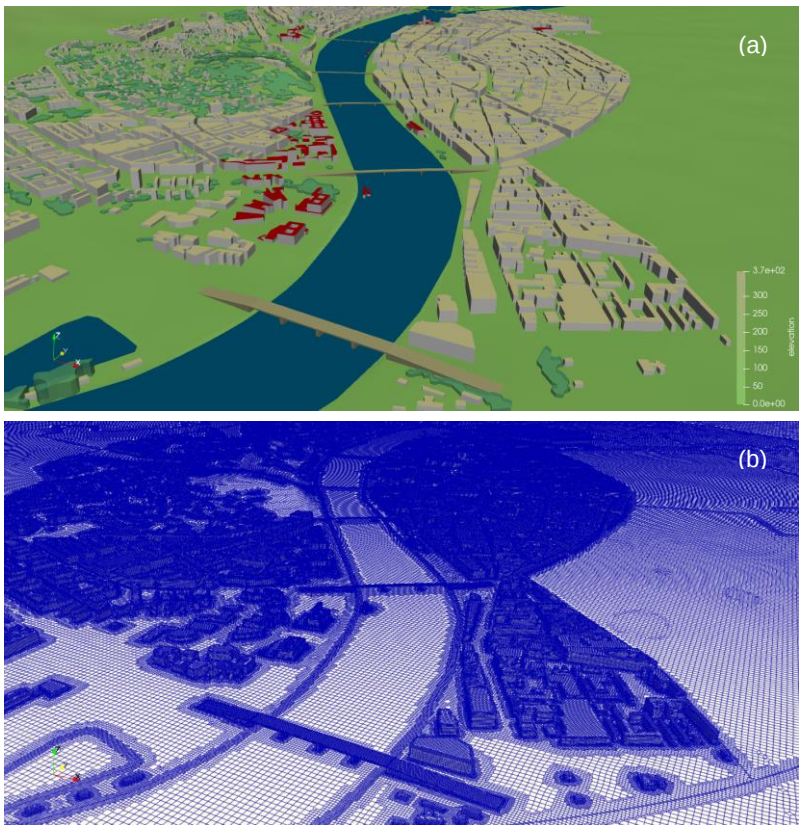

Fig. S1. Axonometric projections on the domain geometry of the exposition area (a) and of the computational surface mesh generated for the same territory (b). The buildings and objects in red are of special interest and were inserted into the domain geometry manually.

The actual numerical simulations were performed in three phases. First, precursor simulations were utilised to determine the initial and lateral boundary conditions. These were actually one-dimensional simulations with a column model to calculate the vertical distributions of velocity

components, turbulent kinetic energy and its dissipation rate based on the measured meteorological data at different heights. As a result, the vertical distributions were imposed as lateral boundary conditions in the next phase. In this, a stationary flow field for the entire geometry was calculated. In the third phase, transient dispersion simulation was carried out using the formerly obtained simulation data for initialising the flow field.

The diameters and masses of each type of pyrotechnic device together with a detailed time schedule of the display in 2021 were made available by the firework provider. The height at which a device explodes was calculated analytically (33 m for a nominal shell diameter of 2.5 cm); (Display Fireworks Manual, 2010). The amounts of particles emitted by the firework explosions were assumed to be proportional to the mass of the pyrotechnic charge. This resulted in a vast number of particles (approximately 1.6×10^{17} kg^{-1}), and, therefore, their numerical simulation is impracticable. The number of emitted particles was taken to be 1 for the smallest charges. As a result, ca. 2.3×10^{6} particles were injected into the computational domain at the time and position corresponding to the detailed schedule of the firework display. In order to make the simulation comparable to the measurements, a linear transformation (scaling to the experimental data) was performed on the simulation results.

Flow simulations generally contain uncertainties arising 1) from the inaccuracy of the initial and boundary conditions (e.g. meteorological data at a single location), 2) from simplifications (geometry modelling errors due to limited spatial resolution), and 3) from approximations applied in physical modelling. Another type of uncertainty is associated with the fact that the spatial positions of the emissions (pyrotechnic explosions as linear or spherical sources), the amount of the emitted particles and their density were approximated. An additional uncertainty factor is related to the limited number of particles that could be tracked in the simulations due to high computational costs. Despite these uncertainties, the time trends of the simulated concentrations and the measured concentrations at the BpART Lab were coherent and similar to each other.

S4. Details of the respiratory deposition modelling and additional results

The following respiratory physiological parameters for a female adult and 5-year-old child performing seated physical activity were adopted: functional residual capacity FRC=2680 and 767 cm^3; tidal volume TV=464 and 213 cm^3; and breathing cycle time CT=4.3 and 2.4 s, respectively (ICRP, 1994). In addition to these respiratory differences, the morphometric data for the child were also rescaled according to age specifically considering the child's height of

110 cm, as suggested by Phalen and Oldham (2001). It was implicitly assumed that the airway structure of the 5-year-old child was already similar to that of adults. The modelled results for males are expected to be similar to that for females (Salma et al., 2002, 2015). Details, properties and the status of the utilised stochastic particle deposition modelling among the other available models were discussed earlier (Asgharian et al., 2009; Hofmann, 2011; and references therein).

There are anatomical, physical and numerical uncertainties in the model due to simplifications. The first group of these simplifications includes, for instance, assumptions on the cylindrical or bent shape of the airways in the bronchial region or regarding the spherical form of the alveoli. The airflow field in the physical model is considered to be laminar and parabolic, with some correction for the turbulent flow in the large bronchial airways. It is very challenging to quantify the effects of these two groups of assumptions. The numerical uncertainties were evaluated and found to be acceptable in a sensitivity analysis of the model (Hofmann and Koblinger, 1990). The overall modelled deposition results agreed reasonably well and satisfactorily with the experimentally obtained data, as demonstrated in several dedicated validation studies (Hofmann et al., 2005; Majid et al., 2011).

Particle number size distributions and total concentrations in the firework plume were utilised in the computations using the electrical mobility diameter representation (Salma et al., 2015). In 2021, three mean particle number size distributions obtained by averaging the three individual spectra before, around the maximum, and well after the firework influence (as detailed in Sect. 3.4.) were utilised as input data for the deposition modelling. The distributions are expected to represent atmospheric conditions under which many spectators were exposed to the firework plume. The depositions were determined by simulating the route and fate of 10^4 inhaled particles.

The respiratory depositions were quantified in terms of deposition fractions, deposition rates and surface density deposition rates. The deposition fraction is the ratio of the number of particles deposited in an airway generation to the number of inhaled particles. The deposition rate is the number of particles deposited in an airway generation in a unit of time. This was calculated as the deposition fraction multiplied by the number of particles inhaled in a unit of time. The latter number was estimated from the measured atmospheric concentration and the breathing parameters as $N_{6–1000}$×TV/CT. The surface density deposition rate is the number of particles deposited in an airway segment in a unit of time per unit of surface area of the segment under consideration. The surface areas of the airway generations were also computed by the

respiratory model (Salma et al., 2002; Balásházy et al., 2007). Adding up the segmental surface area values for the female and the child yielded total lung surface areas of 147 and 128 m^2, respectively, which are in line with morphometric data (Koblinger, 1985).

The deposition probabilities of the particles from the firework smoke were smaller than for atmospheric aerosol (Fig. S2). By integrating the deposition fractions over the ET, TB and AC anatomical regions, the probabilities of 14%, 7% and 25%, respectively were obtained both before and after the fireworks. During the fireworks, the corresponding values altered into 6%, 3% and 14%, respectively. This is due to the considerably larger diameters (203 nm) of the firework particles. For the case of a child, the mean ET and TB deposition fractions before and after the fireworks were similar (14% and 6%, respectively) to those in the case of a female, whereas the deposition fraction in the AC region decreased to half (to 12%). The situation was similar during the firework activity, while the AC deposition fraction was reduced to 6%.

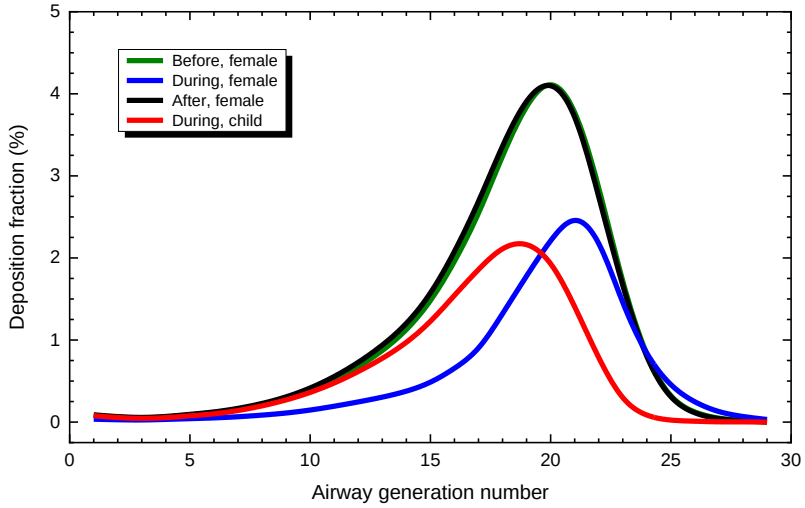

Fig. S2. Deposition fractions (probabilities) of aerosol particles in the airway generations of an adult female performing seated reference physical activity before, during and after the firework influence in 2021. The corresponding distribution for a 5-year-old child during the fireworks is also added.

The peaks of the deposition rate curves (Fig. S3) were realised in the AC anatomical region. The slight difference between the two limiting cases (before and after the fireworks) is explained by the decreasing diurnal tendency in the atmospheric concentration during this time of the day (21:00–23:00) (Salma et al., 2011).

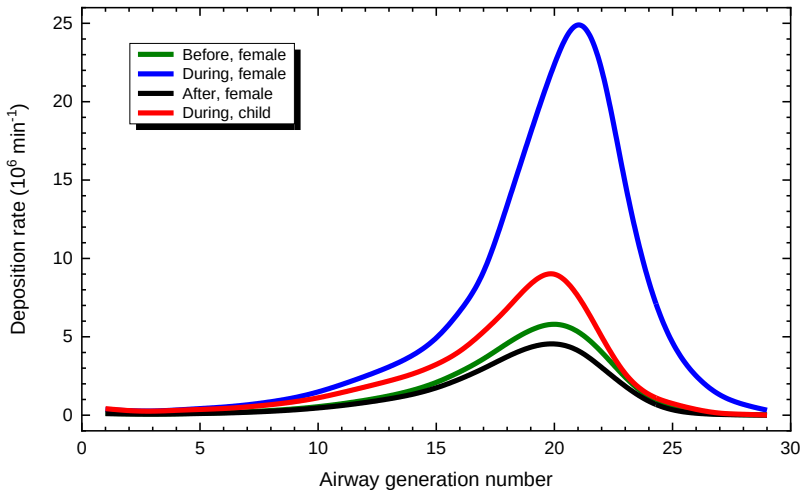

Fig. S3. Deposition rates of aerosol particles in the airway generations of an adult female performing seated reference physical activity before the firework influence (with a particle number concentration of 22×10^3 cm^{-3} measured by the DMPS system), during (156×10^3 cm^{-3}) and after it (17×10^3 cm^{-3}) in 2021. The corresponding distribution for a 5-year-old child during the fireworks is also added.

Table S2. Deposition rates of aerosol particles (in 10^6 min^{-1}) in the extra-thoracic region, tracheobronchial tree and acinar region, in the lungs, and in the total respiratory system of an adult female performing seated physical activity before the firework influence (with a particle number concentration of 22×10^3 cm^{-3} measured by the DMPS system), during (156×10^3 cm^{-3}) and after it (17×10^3 cm^{-3}) in 2021.

Anatomical region	Before	During	After
Extra-thoracic	19	57	16
Tracheobronchial	10	26	8
Acinar	34	146	27
Lung	45	172	36
Respiratory system	63	229	51

The local burden (within the cell environment) has a significant peak in the large central airways (Fig. 6) even if uniform deposition is assumed. The depositions are, however, very inhomogeneous, which further increases the local effects in the carina of these bifurcations (e.g. Farkas et al., 2022). Moreover, the curve for the case of a female during the fireworks extended largely above the other two cases, and this happened in an even more amplified manner for the case of a child. In addition, the high enrichment of transition and heavy metals in the smoke particles (Hickey et al., 2020) makes them extraordinarily hazardous to health. The actual exposures could be higher in hotspot localities occurring downwind from the displays as demonstrated by the smoke dispersion (Fig. 5).

S5. Identification of the firework smoke plume at the fixed measurement site

The firework source areas were to the north of the fixed measurement site in the first approximation (Fig. 1). The flow field around the BpART Lab was studied earlier, and it was found that it is rather complex and that the streamlines depend on the sampling height (Salma et al., 2016). The data in Table S3 suggest that the firework plume in 2014 could not be identified at the BpART Lab most likely due to the calm wind conditions and unfavourable WD (330–342°). In 2015, the wind was stronger, the height of the temperature inversion layer was low, and the direction was not optimal for identifying the plume. In 2016, the deep and stable inversion layer caused the firework smoke to be sporadically detected, even though the actual WD was not optimal. In addition, the particle number concentrations before and after the firework display were higher, which impeded the observation. The differences in WDs between the lower and higher heights were caused by the sublocal modifying effects of the neighbouring buildings (Salma et al., 2016). In 2021, 2022 and 2017, almost all meteorological conditions favoured detection. In 2017, the WS was above the average, which resulted in a shorter duration. In 2021 and 2022, a stronger temperature inversion, a lower WS and the powerful firework activity caused a dense plume at the BpART Lab.

Table S3. Mean air temperature (*T*), relative humidity (RH), wind speed (WS) and wind direction (WD) at the BpART Lab (at a height of 13 m above street level) and the mean WS and WD data above the rooftop level of the building complex (at 42 m) for 21:00–22:00 LDST on 20 August 2014, 2015, 2016, 2017, 2020, 2021 and 2022. The WS and WD data at the top of the temperature inversion layer (TIL) and the height of the TIL (*h* in m) was obtained using radiosonding at 24:00 UTC. The fireworks were postponed in 2022 from 20 to 27 August.

Year	*T* (°C)	RH (%)	WS (m s^{-1})			WD (°)		
			at 13 m	at 42 m	at TIL (*h*)	at 13 m	at 42 m	at TIL
2014	19	88	0.3	0.5	1.5 (191)	262	342	330
2015	18	84	2.0	4.3	7 (110)	5	45	35
2016	25	77	0.9	1.0	2 (226)	180	192	165
2017	20	53	3.4	4.2	4 (148)	332	357	5
2020	24	58	0.9	2.1	1 (176)	254	298	10
2021	22	61	0.4	0.3	1.5 (190)	233	350	350
2022	28	46	2.1	3.2	7 (343)	250	15	110

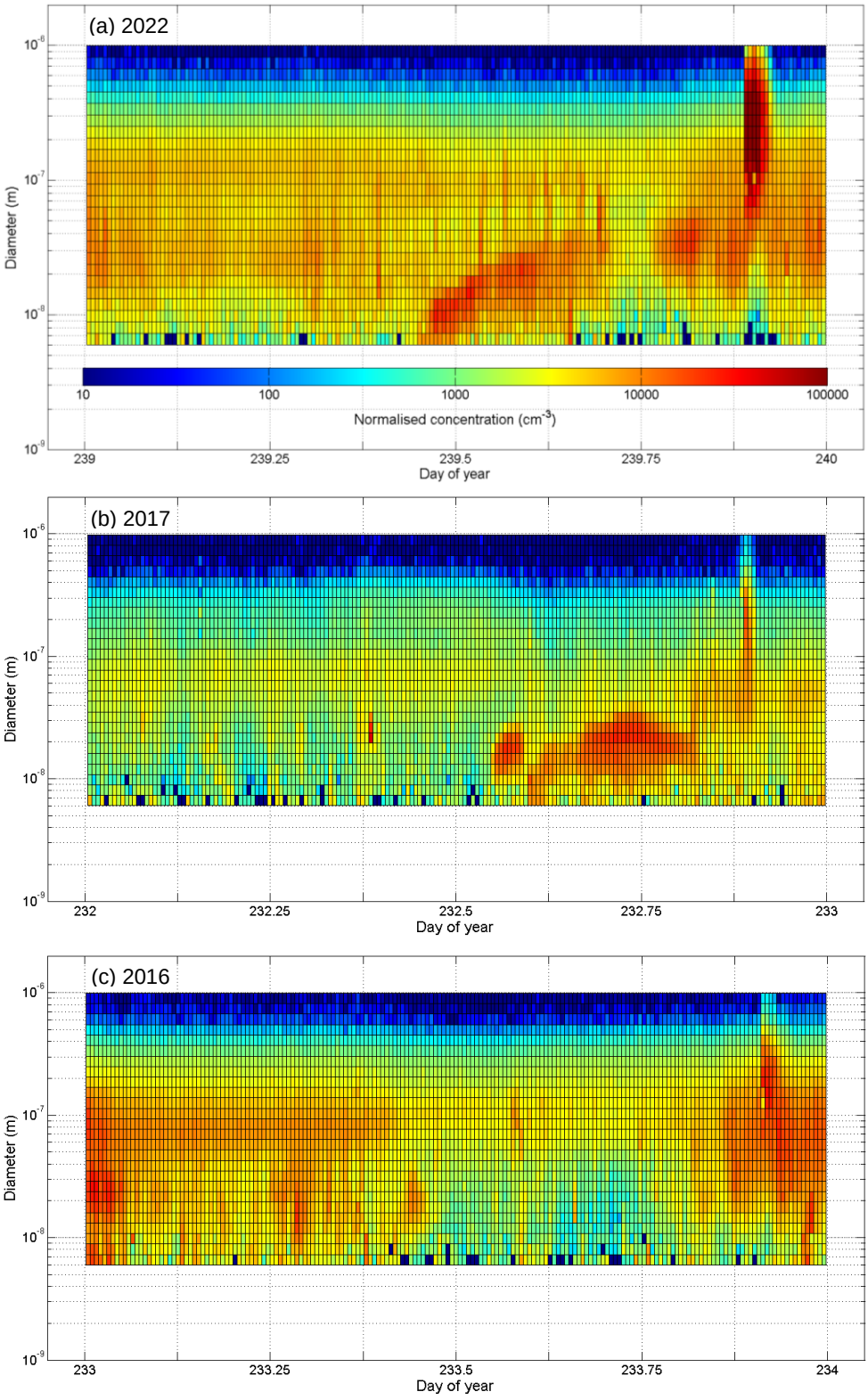

Fig. S4. Contour plots of particle number size distributions in the diameter range from 6 to 1000 nm on 20 August 2022 (a), 2017 (b) and 2016 (c). The contour plot for 2021 is shown in Fig. 2. The fireworks were postponed in 2022 from 20 to 27 August. The firework displays started at 21:00 LDST and lasted for ca. 30 min. In these years, the firework plume was evidently identified at the BpART Lab. It appears as a dark red oval patch in the right upper part of the figures. There were two weak new particle formation and growth events in form of banana curves starting at 10:30 in 2022 and at 14:15 in 2017.

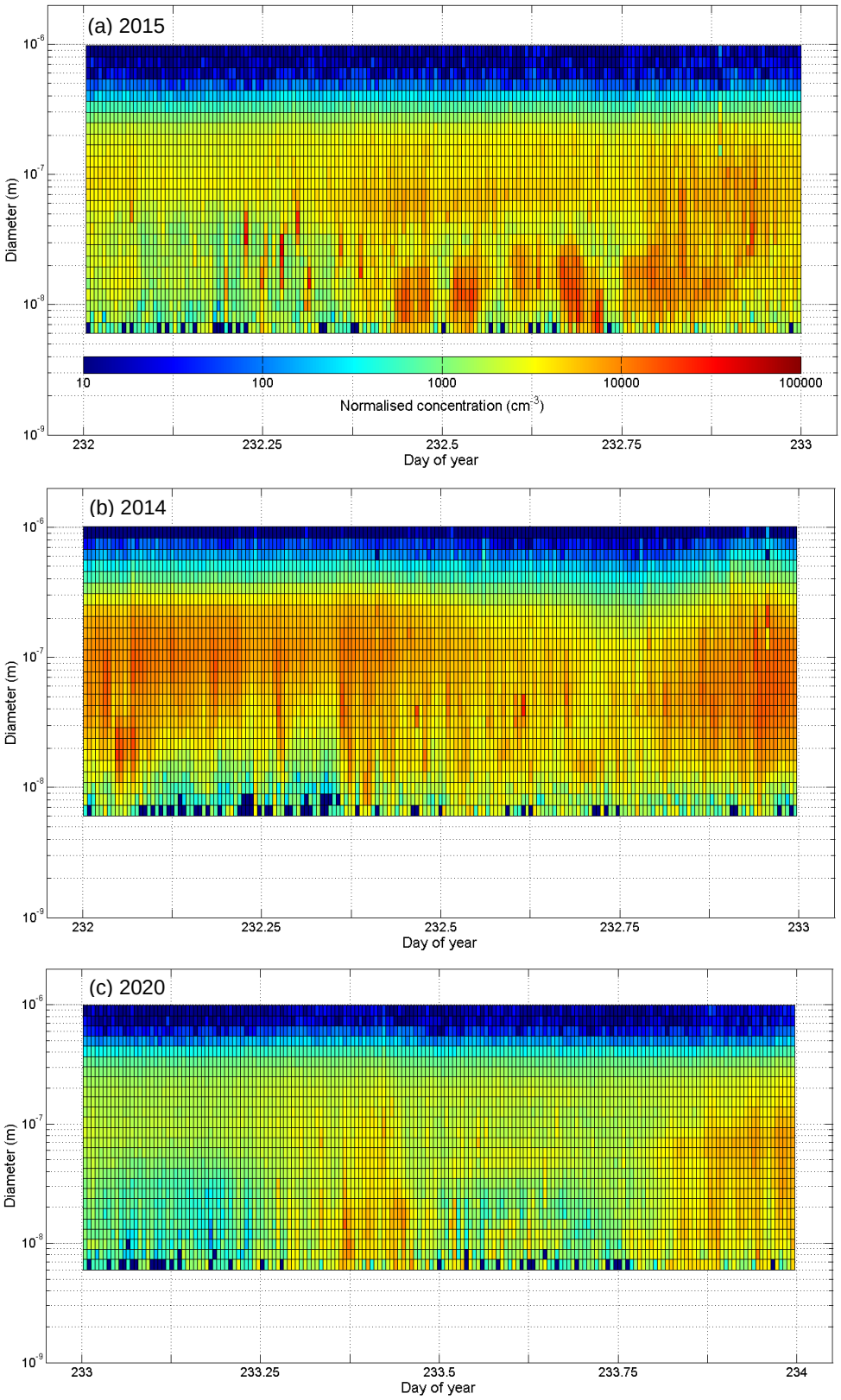

Fig. S5. Contour plots of particle number size distributions in the diameter range from 6 to 1000 nm on 20 August for the years when the firework plume could not be obviously identified at the BpART Lab, thus in 2015 (a) and 2014 (b). The firework displays started at 21:00 LDST and lasted for ca. 30 min. In 2020 (c), there were no fireworks, and it was included into the study for checking and verification purposes.

S6. Time series of particle number concentration, size distribution, condensation sink and coagulation sink

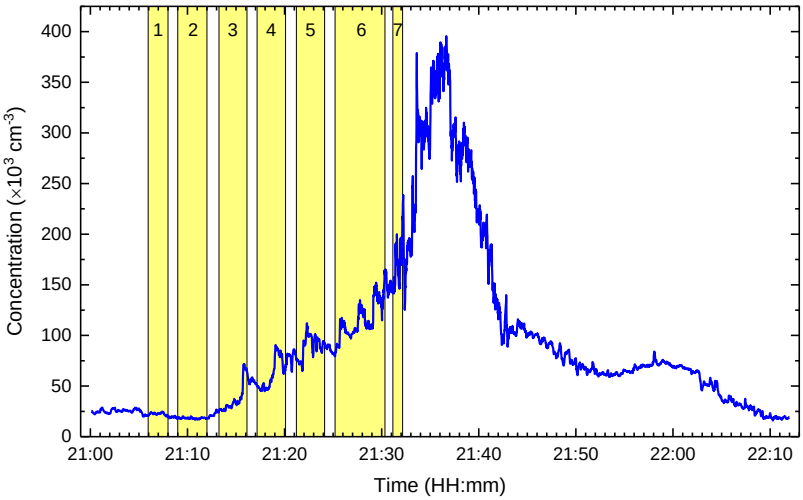

Fig. S6. Time schedule of the firework displays and time series of total particle number concentration measured by CPC with a resolution of 1 s at the BpART Lab on 20 August 2021. The yellow bands 1–7 indicate the firework activity. The counts of the deployed firework effects were 2574, 5326, 2740, 5110, 4749, 12015 and 2000, respectively. Activities 1–6 represent explosions mostly in the air (including Roman candles which emit larger numbers of particles during the elevation of the missiles) at heights up to 300 m, whereas activity 7 was a so-called waterfall (Greek) firework from the pavement level of the Elisabeth and Liberty Bridges down to the surface of the Danube over a horizontal extension of 200 m.

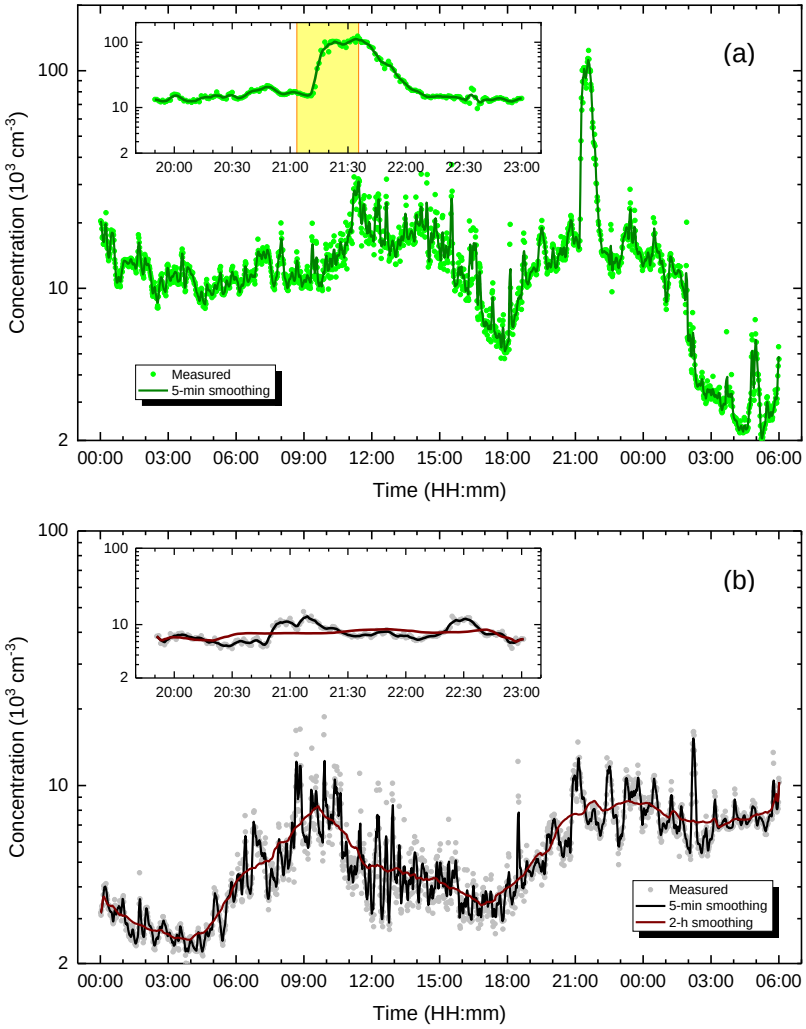

Fig. S7. Time series of total particle number concentration measured by CPC with a resolution of 1 min on 27 and 28 August 2022 (a) and on 20 and 21 August 2020 (b) together with their 5-min smoothing. For 2020, 2-h smoothing is also displayed to mark the diurnal pattern of the concentration. In 2022 the fireworks were postponed from 20 to 27 August. The firework activity started at 21:03 and lasted for 33 min. There were no fireworks in 2020, and it was included into the study for checking and verification purposes. The inserts show a more detailed time evolution between 19:50 and 23:00 and the firework activity in 2022 is indicated with a yellow band.

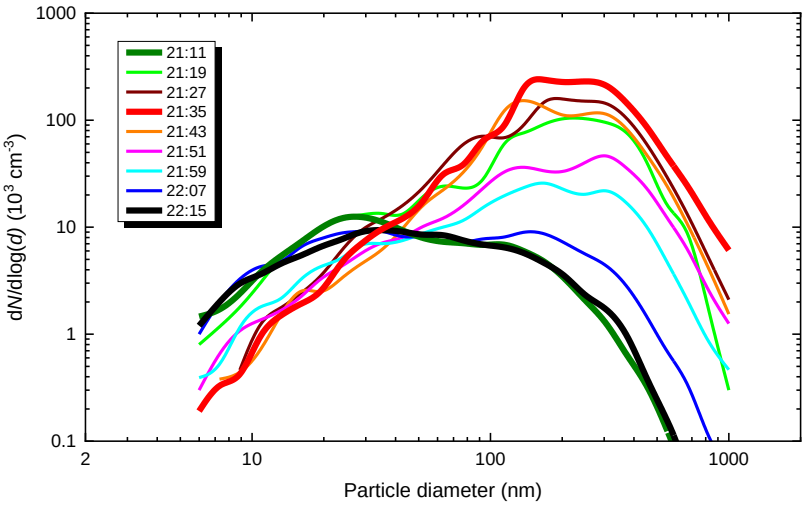

Fig. S8. Time series of the particle number size distribution from 21:11 to 22:15 for the fireworks in 2022. The distributions just before the observed firework activity (21:11), at its concentration maximum (21:35) and after it settled down to the levels before the show (22:15) are emphasised in thicker curves. The timing data refer to the end time of the 8-min measuring cycle of the DMPS system.

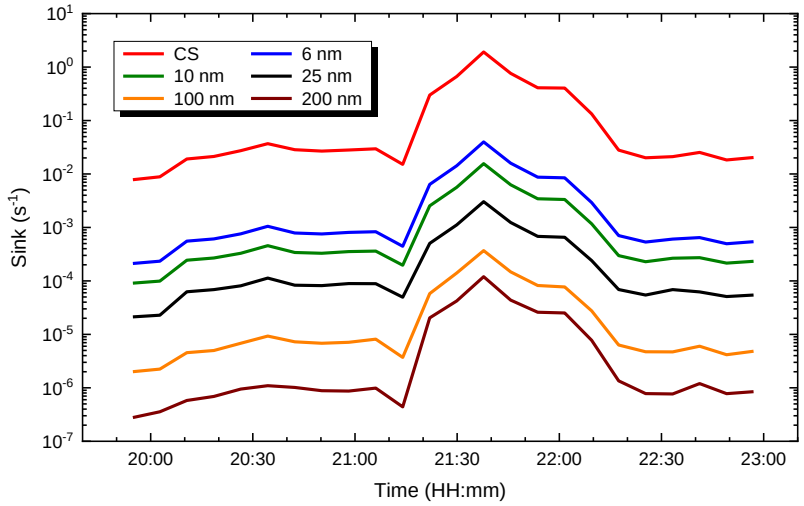

Fig. S9. Time series of condensation sink (CS) and coagulation sinks for particles with a diameter of 6, 10, 25, 100 and 200 nm for the firework display in 2021.

S7. Details of the exponential decay curve analysis

It was assumed that: 1) the main sink could be expressed by first order kinetics, 2) the dispersion of the firework plume to the measurement site was continuous and constant, and 3) it caused constant and identical dilution of the smoke over a certain time interval of interest. The assumptions represent acceptable approximations to reality during the events and under the actual atmospheric conditions (Sect. 3.5.). The concentrations $N_{100–1000}$ were considered for this purpose as the most sensitively impacted size range. Those time spans were selected for the

evaluations during which the log($N_{100–1000}$) dependency on time after its maximum could be considered to be linear. This comprised 35–45 min (4–6 DMPS data points).

S8. Details on the upper diameter for PM mass conversion

Particle number size distributions were converted to PM mass, and these were compared to each other to assess the relative effects of the fireworks in terms of mass concentration. Spherical particles with a density of ρ =1.7 g cm^{-3} were assumed (Zhang et al., 2010; Wehner et al., 2020). It can be derived using the Hatch-Choate conversion equation (Seinfeld and Pandis, 1998) adopting the ρ and actual GSD (Table 1) that the fireworks NMMD of 200 nm corresponds to 0.8 µm mass median mobility diameter (MMMD). Furthermore, it can be calculated using the relationship (DeCarlo et al., 2004; Khlystov et al., 2004)

$$d_{\mathrm{a}} = \sqrt{\frac{\rho}{\rho_0}\frac{1}{\chi}\frac{C_{\mathrm{c}}(d_{\mathrm{ve}})}{C_{\mathrm{c}}(d_{\mathrm{a}})}}\, d_{\mathrm{ve}} \qquad \text{(S1)}$$

that the corresponding aerodynamic diameter (d_{a} or MMAD, mass median aerodynamic diameter) is larger than this electric mobility equivalent diameter by a factor of approximately f=2. In Eq. S1, d_{ve} is volume equivalent diameter, ρ_0 is unit density (ρ_0=1 g cm^{-3}), χ is the dynamic shape factor of the particle, and $C_{\mathrm{c}}(d)$ is the slip correction factor for the particle with a diameter of d. It was assumed that the particles have a spherical shape, which implies that χ=1 by definition, and that d_{ve} equals to the electric mobility diameter (Salma et al., 2015).

Considering that the GSD for the mass size distribution is equal to that of the particle number, it is expected that the mass size distribution in aerodynamic diameter representation spreads substantially toward larger diameters. Assuming lognormal distribution of concentrations, 95% of mass data are expected to belong to the diameter interval from MMMD×f/GSD^2 to MMMD×f×GSD^2. Hence, the upper size of the interval is at 0.8×2×1.7^2=4.6 µm. This set of arguments and the estimated result are in line with measured mass size distributions of firework-related chemical elements (Tanda et al., 2019). All these jointly indicate that the converted PM mass from the particle number size distributions corresponds to the PM_{10} size fraction with some possible underestimation.

Similar conversions into partial PM mass size fractions are expected to yield larger relative uncertainties mainly due to the differences between the two types of size distribution and of the equivalent diameters and to the varying particle density with size.

References

Asgharian, B., Price, O., Miller, F., Subramaniam, R., Cassee, F. R., Freijer, J., van Bree, L., Winter-Sorkina, R.: Multiple-path particle dosimetry model (MPPD v 2.11): A model for human and rat airway particle dosimetry, Hamner Institutes for Health Sciences, National Institute for Public Health and the Environment and Ministry of Housing, Spatial Planning and the Environment, Raleigh, North Carolina, USA, 2009.

Balásházy, I., Alföldy, B., Molnár, A. J., Hofmann, W., Szőke, I., Kis, E.: Aerosol drug delivery optimization by computational methods for the characterization of total and regional deposition of therapeutic aerosols in the respiratory system, Curr. Comput. Aided Drug Des., 3, 13–32, https://doi.org/10.2174/157340907780058727, 2007.

Balogh, M. and Kristóf, G.: Fine scale simulation of turbulent flows in urban canopy layers, Időjárás, 114, 135–148, 2010.

Barman, S. C., Singh, R., Negi, M. P., Bhargava, S. K.: Ambient air quality of Lucknow City (India) during use of fireworks on Diwali festival, Environ. Monit. Assess., 137, 495–504, https://doi.org/10.1007/s10661-007-9784-1, 2008.

Bossard, M., Feranec, J., Otahel, J.: CORINE land cover technical guide – addendum 2000, European Environment Agency, Copenhagen, 2000.

Burki, T. K.: Are fireworks a hazard for respiratory health?, Lancet, 5, 103–104, https://doi.org/10.1016/S2213-2600(17)30016-4, 2017.

Cao, X., Zhang, X., Tong, D. Q., Chen, W., Zhang, S., Zhao, H., Xiu, A.: Review on physicochemical properties of pollutants released from fireworks: environmental and health effects and prevention, Environ. Rev., 26, 133–155, https://doi.org/10.1139/er-2017-0063, 2018.

Copernicus Land Monitoring, Urban Atlas, https://land.copernicus.eu/pan-european/corine-land-cover/clc2018, last accessed on 14 October 2021, 2018a.

Copernicus Land Monitoring, Corine Land Cover, https://land.copernicus.eu/local/urban-atlas/urban-atlas-2018, last accessed on 14 October 2021, 2018b.

DeCarlo, P. F., Slowik, J. G., Worsnop, D. R., Davidovits, P., Jimenez, J. L.: Particle morphology and density characterization by combined mobility and aerodynamic diameter measurements. Part 1: Theory, Aerosol Sci. Technol., 38, 1185–1205, https://doi.org/10.1080/027868290903907, 2004.

De Meij, A. and Vinuesa, J. F.: Impact of SRTM and Corine Land Cover data on meteorological parameters using WRF, Atmos. Res., 143, 351–370, https://doi.org/10.1016/j.atmosres.2014.03.004, 2014.

Dickerson, A. S., Benson, A. F., Buckley, B., Chan, E. A. W.: Concentrations of individual fine particulate matter components in the USA around July 4th, Air Qual. Atmos. Health, 10, 349–358, https://doi.org/10.1007/s11869-016-0433-0, 2017.

Display Fireworks Manual, Explosive Regulatory Division of Natural Resources, Ottawa, Canada, ISBN 978-1-100-15117-5, 2010.

Farkas, Á., Füri, P., Thén, W., Salma, I.: Effects of hygroscopic growth of urban aerosol particles on their modelled regional and local deposition in healthy and COPD-compromised human respiratory system, Sci. Total Environ., 806, 151202, https://doi.org/10.1016/j.scitotenv.2021.151202, 2022.

Gao, H., Shi, J., Cheng, H., Zhang, Y., Zhang, Y.: The impact of long- and short-term exposure to different ambient air pollutants on cognitive function in China, Environ. Internat., 151, 106416, https://doi.org/10.1016/j.envint.2021.106416, 2021.

Godri, K. J., Green, D. C., Fuller, G. W., Dall'Osto, M., Beddows, D. C., Kelly, F. J., Harrison, R. M., Mudway, I. S.: Particulate oxidative burden associated with firework activity, Environ. Sci. Technol., 44, 8295–8301, https://doi.org/10.1021/es1016284, 2010.

Greven, F. E., Vonk, J. M., Fischer, P., Duijm, F., Vink, N. M., Brunekreef, B.: Air pollution during New Year's fireworks and daily mortality in the Netherlands, Sci. Rep., 9, 5735, https://doi.org/10.1038/s41598-019-42080-6, 2019.

Harrison, R. M., Bousiotis, D., Mohorjy, A. M., Alkhalaf, A. K., Shamy, M., Alghamdi, M., Khoder, M., Costa, M.: Health risk associated with airborne particulate matter and its components in Jeddah, Saudi Arabia, Sci. Total Environ., 590–591, 531–539, https://doi.org/10.1016/j.scitotenv.2017.02.216, 2017.

Harrison, R. M. and Yin, J.: Particulate matter in the atmosphere: Which particle properties are important for its effects on health?, Sci. Total Environ., 249, 85–101, https://doi.org/10.1016/S0048-9697(99)00513-6, 2000.

Hasager, C. B., Nielsen, N. N., Jensen, N. O., Boegh, E., Christensen, J. H., Dellwik, E., Soegaard, H.: Effective roughness calculated from satellite-derived land cover maps and hedge-information used in a weather forecasting model, Bound-Lay. Meteorol., 109, 227–254, https://doi.org/10.1023/A:1025841424078, 2003.

Hickey, C., Gordon, C., Galdanes, K., Blaustein, M., Horton, L., Chillrud, S., Ross, J., Yinon, L., Chen, L. Ch., Gordon, T.: Toxicity of particles emitted by fireworks, Part. Fibre Toxicol., 17, 28, https://doi.org/10.1186/s12989-020-00360-4, 2020.

Hirai, K., Yamazaki, Y., Okada, K., Furuta, S., Kubo, K.: Acute eosinophilic pneumonia associated with smoke from fireworks, Int. Med., 39, 401–403, https://doi.org/10.2169/internalmedicine.39.401, 2000.

Hoek, G., Dockery, D. W., Pope, A., Neas, L., Roemer, W., Brunekreef, B.: Association between PM_{10} and decrements in peak expiratory flow rates in children: reanalysis of data from five panel studies, Eur. Respir. J., 11, 1307–1311, https://doi.org/10.1183/09031936.98.11061307, 1998.

Hofmann, W. and Koblinger, L.: Monte Carlo modeling of aerosol deposition in human lungs, Part II: Deposition fractions and their sensitivity to parameter variations, J. Aerosol Sci., 21, 675–688, https://doi.org/10.1016/0021-8502(90)90122-E, 1990.

Hofmann, W., Sturm, R., Fleming, J. S., Conway, J. H., Bolt, L.: Simulation of three-dimensional particle deposition patterns in human lungs and comparison with experimental SPECT data, Aerosol Sci. Technol., 39, 771–781, https://doi.org/10.1080/02786820500237158, 2005.

Hofmann, W.: Modelling inhaled particle deposition in the human lung – a review, J. Aerosol Sci., 42, 693–724, https://doi.org/10.1016/j.jaerosci.2011.05.007, 2011.

ICRP (International Commission on Radiological Protection), Publication 66, Human respiratory tract model for radiological protection, Annals of the ICRP 24, Pergamon Press, Oxford, UK, 1994.

Jancewicz, K.: Remote sensing data in wind velocity field modeling: a case study from the Sudetes (SW Poland), Pure Appl. Geophys., 171, 941–964, https://doi.org/10.1007/s00024-013-0698-2, 2014.

Joly, A., Smargiassi, A., Kosatsky, T., Fournier, M., Zlotorzynska, D. E., Celo, V., Mathieu, D., Servranckx, R., D'amours, R., Malo, A., Brook, J.: Characterization of particulate exposure during fireworks displays, Atmos. Environ., 44, 4325–4329, https://doi.org/10.1016/j.atmosenv.2009.12.010, 2010.

Khlystov, A., Stanier, C., Pandis, S. N.: An algorithm for combining electrical mobility and aerodynamic size distributions data when measuring ambient aerosol, Aerosol Sci. Technol., 38, 229–238, https://doi.org/10.1080/02786820390229543, 2004.

Koblinger, L.: Analysis of human lung morphometric data for stochastic aerosol deposition calculations, Phys. Med. Biol., 30, 541–556, https://doi.org/10.1088/0031-9155/30/6/004, 1985.

Li, L., Hu, D., Zhang, W., Cui, L., Jia, X., Yang, S., Liu, S., Deng, F., Liu, J, Guo, X.: Effect of short-term exposure to particulate air pollution on heart rate variability in normal-weight and obese adults, Environ. Health, 20, 29, https://doi.org/10.1186/s12940-021-00707-0, 2021.

Lin, Ch-Ch.: A review of the impact of fireworks on particulate matter in ambient air, J. Air Waste Manage. Assoc., 66, 1171–1182, https://doi.org/10.1016/10.1080/10962247.2016.1219280, 2016.

Majid, H., Hofmann, W., Winkler-Heil, R.: Comparison of stochastic lung deposition fractions with experimental data, Ann. Occup. Hyg., 56, 278–291, https://doi.org/10.1093/annhyg/mer100, 2011.

Matsuo, R., Michikawa, T., Ueda, K., Ago, T., Nitta, H., Kitazono, T., Kamouchi, M., Fukuoka Stroke Registry Investigators: Short-term exposure to fine particulate matter and risk of ischemic stroke, Stroke, 47, 3032–3034, https://doi.org/10.1161/STROKEAHA.116.015303, 2016.

Moreno, T., Querol, X., Alastuey, A., Minguillòn, M. C., Pey, J., Rodriguez, S., Mirò, J. V., Felis, C., Gibbons, W.: Recreational atmospheric pollution episodes: Inhalable metalliferous particles from firework displays, Atmos. Environ., 41, 913–22, https://doi.org/10.1016/j.atmosenv.2006.09.019, 2007.

Moreno, T., Querol, X., Alastuey, A., Amato, F., Pey, J., Pandolfi, M., Kuenzli, N., Bouso, L., Rivera, M., Gibbons, W.: Effect of fireworks events on urban background trace metal aerosol concentrations: is the cocktail worth the show?, J. Hazard. Mater., 183, 945–949, https://doi.org/10.1016/j.jhazmat.2010.07.082, 2010.

Mousavi, A., Yuan, Y., Masri, S., Barta, G., Wu, J.: Impact of 4th of July fireworks on spatiotemporal $PM_{2.5}$ concentrations in California based on the PurpleAir Sensor Network: implications for policy and environmental justice, Int. J. Environ. Res. Public Health, 18, 5735, https://doi.org/10.3390/ijerph18115735, 2021.

OpenStreetMap Foundation, OSM Buildings, https://osmbuildings.org., last accessed on 16 January 2022, 2021.

Orellano, P., Reynoso, J., Quaranta, N., Bardach, A., Ciapponi, A.: Short-term exposure to particulate matter (PM_{10} and $PM_{2.5}$), nitrogen dioxide (NO_2), and ozone (O_3) and all-cause and cause-specific mortality: systematic review and meta-analysis, Environ. Internat., 142, 105876, https://doi.org/10.1016/j.envint.2020.105876, 2020.

Park, J., Sohn, J. H., Cho, S. J., Seo, H. Y., Hwang, I-U., Hong, Y-Ch., Kim, K-N.: Association between short-term air pollution exposure and attention-deficit/hyperactivity disorder-related hospital admissions among adolescents: A nationwide time-series study, Environ. Pollut., 266, 115369, https://doi.org/10.1016/j.envpol.2020.115369, 2020.

Phalen, R. F. and Oldham, M. J.: Methods for modeling particle deposition as a function of age, Resp. Physiol., 128, 119–130, https://doi.org/10.1016/S0034-5687(01)00270-5, 2001.

Pirker, L., Velkavrh, Ž., Osīte, A., Drinovec, L., Močnik, G., Remškar, M.: Fireworks – a source of nanoparticles, $PM_{2.5}$, PM_{10}, and carbonaceous aerosols, Air Qual. Atmos. Health, https://doi.org/10.1007/s11869-021-01142-3, 2021.

Potapov, P., Li, X., Hernandez-Serna, A., Tyukavina, A., Hansen, M. C., Kommareddy, A., Pickens, A., Turubanova, S., Tang, H., Silva, C. E., Armston, J., Dubayah, R., Blair, J. B., Hofton, M.: Mapping and monitoring global forest canopy height through integration of GEDI and Landsat data, Remote Sens. Environ., 112165, https://doi.org/10.1016/j.rse.2020.112165, 2020.

Russell, M. S.: The chemistry of fireworks, The Royal Society of Chemistry, Cambridge, UK, 2009.

Salma, I., Balásházy, I., Hofmann, W., Záray, Gy.: Effect of physical exertion on the deposition of urban aerosols in the human respiratory system, J. Aerosol Sci., 33, 983–997, https://doi.org/10.1016/S0021-8502(02)00051-4, 2002.

Salma, I., Borsós, T., Weidinger, T., Aalto, P., Hussein, T., Dal Maso, M., Kulmala, M.: Production, growth and properties of ultrafine atmospheric aerosol particles in an urban environment, Atmos. Chem. Phys., 11, 1339–1353, https://doi.org/10.5194/acp-11-1339-2011, 2011.

Salma, I., Füri, P., Németh, Z., Farkas, Á., Balásházy, I., Hofmann, W., Farkas, Á.: Lung burden and deposition distribution of inhaled atmospheric urban ultrafine particles as the first step in their health risk assessment, Atmos. Environ., 104, 39–49, https://doi.org/10.1016/j.atmosenv.2014.12.060, 2015.

Salma, I., Németh, Z., Weidinger, T., Kovács, B., Kristóf, G.: Measurement, growth types and shrinkage of newly formed aerosol particles at an urban research platform, Atmos. Chem. Phys., 16, 7837–7851, https://doi.10.5194/acp-16-7837-2016, 2016.

Sarkar, S., Khillare, P. S., Jyethi, D. S., Hasan, A., Parween, M.: Chemical speciation of respirable suspended particulate matter during a major firework festival in India, J. Haz. Mat., 184, 321–330, https://doi.org/10.1016/j.jhazmat.2010.08.039, 2010.

Schwartz, J., Coull, B., Laden, F., Ryan, L.: The effect of dose and timing of dose on the association between airborne particles and survival, Environ. Health Perspect., 116, 64–69, https://doi.org/10.1289/ehp.9955, 2008.

Seidel, D. J. and Birnbaum, A. N.: Effects of Independence Day fireworks on atmospheric concentrations of fine particulate matter in the United States, Atmos. Environ., 115, 192–198, https://doi.org/10.1016/j.atmosenv.2015.05.065, 2015.

Seinfeld, J. H. and Pandis, S. N.: Atmospheric chemistry and physics: from air pollution to climate change, Wiley, Hoboken, USA, 1998.

Shehab, M. A. and Pope, F. D.: Effects of short-term exposure to particulate matter air pollution on cognitive performance, Sci. Rep., 9, 8237, https://doi.org/10.1038/s41598-019-44561-0, 2019.

Shi, L., Zanobetti, A., Kloog, I., Coull, B. A., Koutrakis, P., Melly, S. J., Schwartz, J. D.: Low-concentration $PM_{2.5}$ and mortality: estimating acute and chronic effects in a population-based study, Environ. Health Perspect., 124, 46–52, https://doi.org/10.1289/ehp.1409111, 2016.

Silva, J., Ribeiro, C., Guedes, C.: Roughness length classification of Corine Land Cover Classes, in: Proceedings of the European Wind Energy Conference, 7–10 May 2007, Milan, Italy, 2007.

Singh, A., Pant, P., Pope, F. D.: Air quality during and after festivals: Aerosol concentrations, composition and health effects, Atmos. Res., 227, 220–232, https://doi.org/10.1016/j.atmosres.2019.05.012, 2019.

Sun, Y., Han, Z., Du, Z., Li, Z., Cong, X.: Preparation and performance of environmental friendly sulphur-free propellant for fireworks, Appl. Therm. Eng., 126, 987–996, https://doi.org/10.1016/j.applthermaleng.2017.08.003, 2017.

Tanda, S., Ličbinský, R., Hegrová, J., Goessler, W.: Impact of New Year's Eve fireworks on the size resolved element distributions in airborne particles, Environ. Internat., 128, 371–378, https://doi.org/10.1016/j.envint.2019.04.071, 2019.

Tasmin, S., Ng, C. F. S., Stickley, A., Md, N., Saroar, G., Yasumoto, S., Watanabe, C.: Effects of short-term exposure to ambient particulate matter on the lung function of school children in Dhaka, Bangladesh, J. Epidemiol., 30, S15–S23, https://doi.org/10.1097/EDE.0000000000001012, 2019.

Vecchi, R., Bernardoni, V., Cricchio, D., D'Alessandro, A., Fermo, P., Lucarelli, F., Nava, S., Piazzalunga, A., Valli, G.: The impact of fireworks on airborne particles, Atmos. Environ., 42, 1121–32, https://doi.org/10.1016/j.atmosenv.2007.10.047, 2008.

Wehner, B., Wiedensohler, A., Heintzenberg, J.: Submicrometer aerosol size distributions and mass concentration of the Millennium fireworks 2000 in Leipzig, Germany, J. Aerosol Sci., 31, 1489–1493, https://doi.org/10.1016/S0021-8502(00)00039-2, 2000.

Yao, L., Wang, D., Fu, Q., Qiao, L., Wang, H., Li, L., Sun, W., Li, Q., Wang, L., Yang, X., Zhao, Z., Kan, H., Xian, A., Wang, G., Xiao, H., Chen, J.: The effects of firework regulation on air quality and public health during the Chinese Spring Festival from 2013 to 2017 in a Chinese megacity, Environ. Internat., 126, 96–106, https://doi.org/10.1016/j.envint.2019.01.037, 2019.

Zhang, M., Wang, X., Chen, J., Cheng, T., Wang, T., Yang, X., Gong, Y., Geng, F., Chen, Ch.: Physical characterization of aerosol particles during the Chinese New Year's firework events, Atmos. Environ., 44, 5191–5198, https://doi.org/10.1016/j.atmosenv.2010.08.048, 2010.